Two-Dimensional Index Modulation for the Large-Scale Multi-User MIMO Uplink

Siyao Lu, Mohammed El-Hajjar, *Senior Member, IEEE* and Lajos Hanzo, *Fellow, IEEE*

***Abstract*—A novel compressed sensing-aided generalised space-frequency index modulation (CS-GSFIM) scheme is conceived for the large-scale multi-user multiple-input multiple-output uplink (LS-MU-MIMO-UL). Explicitly, the information bits are mapped both to the spatial- and frequency-domain indices, where we treat the activation patterns of the transmit antennas (TAs) and of the subcarriers separately. Specifically, our indexing strategy strikes a flexible trade-off between the throughput (Tp), performance and complexity. In order to further increase the system's achievable rate, CS-aided pre-processing is applied to the subcarriers. An upper bound of the average bit error probability (ABEP) of the proposed system using the optimal maximum likelihood (ML) detector is derived, which is shown to be tight by our simulation results at moderate to high signal-to-noise ratios (SNRs). Then we design a CS-aided reduced-complexity detector, namely the reduced search-space based iterative matching pursuit (RSS-IMP), which significantly reduces the detection complexity compared to the ML detection and makes the proposed design a feasible one for LS-MU scenarios. Furthermore, the simulation results presented in this paper demonstrate that the proposed RSS-IMP detector significantly reduces the detection complexity, while attaining better performances than both the conventional MU-MIMO-OFDM system using the ML detector and the proposed system using the minimum mean square error (MMSE) detector. We also characterise the performances of the proposed system in the presence of channel estimation errors. Our simulation results show that the proposed CS-GSFIM system is more robust to imperfect channel than the conventional MU-MIMO-OFDM system. In order to achieve a near-capacity performance, soft-input soft-output (SISO) decoders are designed for the proposed CS-GSFIM system using both the ML and the RSS-IMP multi-user detectors (MUDs) for detecting all users.**

***Index Terms*—Two-Dimensional Index Modulation, Large-Scale Multiple-Input Multiple-Output (MIMO) System, Compressed Sensing, Orthogonal Frequency Division Multiplexing (OFDM), Near-Capacity Performance, Maximum Achievable Rate, Low-Complexity Detector.**

I. Introduction

MULTIPLE-INPUT multiple-output orthogonal frequency-division multiplexing (MIMO-OFDM) has attracted substantial interest as a benefit of its high spectral efficiency (SE) and robustness in frequency-selective channel conditions [1]. Large-scale multi-user MIMO (LS-MU-MIMO) systems [2] benefit from further improved spectral and power efficiencies in the context of next generation wireless systems.

Spatial modulation (SM) has the extra appeal that the number of radio frequency (RF) chains may be flexibly adjusted [3]. In its simplest form, only one out of multiple transmit antennas (TAs) is active and the other TAs remain silent at any time instant, where a symbol chosen from a constellation diagram will be transmitted on the activated TA [3], [4]. Therefore, the fundamental principle of SM may be viewed as an extension of signal constellations to a new dimension, which is the spatial dimension (SD). Furthermore, in order to strike more flexible trade-offs, generalised SM (GSM) was proposed for simultaneously activating multiple TAs at a time [5]. Then GSM was invoked in the uplink (UL) of LS-MU-MIMO systems [6], where a message passing based low-complexity detector was also proposed.

Inspired by the idea of SM, index modulation aided OFDM (OFDM-IM) was proposed for frequency-selective fading channels [7], where the information is conveyed by both the classic amplitude/phase modulated (APM) symbols and by the index of the activated subcarriers [8], [9]. In order to further increase the SE and the energy efficiency (EE) of OFDM-IM systems, a compressed sensing (CS) assisted signalling strategy was proposed for OFDM-IM systems in [10]–[12]. Additionally, OFDM-IM designed for the MU UL and downlink (DL) was proposed in [13], where the peak to average power ratio (PAPR) of the classical MU-OFDM system was reduced.

Furthermore, multi-dimensional IM schemes were proposed in [14]–[18], where it was shown that, for a given rate, improved performance may be achieved upon increasing the number of indexed transmission entities. Specifically, in [18] a multi-dimensional IM scheme was proposed for single-user scenarios relying both on frequency-domain as well as on spatial-domain IM for attaining an improved performance compared both to conventional MIMO-OFDM systems and to one-dimensional IM systems. Explicitly, in [18] the distinctive combination of active TAs remains fixed in each OFDM subcarrier group, whilst in this contribution it was configured for increasing the system's flexibility. Applying the multi-dimensional IM strategy in LS-MU-MIMO systems is promising. However, one of the most challenging tasks in LS-MU-MIMO systems is the design of a reliable, low-complexity multi-user detector (MUD) for employment at the base station (BS).

It was predicted by Shannon [19] that forward error correction (FEC) coding can be used to attain a reliable communication, whilst incorporating redundancy into the transmitted

L. Hanzo would like to acknowledge the financial support of the EPSRC projects EP/Noo4558/1, EP/PO34284/1, COALESCE, of the Royal Society's Global Challenges Research Fund Grant as well as of the European Research Council's Advanced Fellow Grant QuantCom.

The authors are with the School of Electronics and Computer Science, University of Southampton, Southampton SO17 1BJ, U.K. (e-mail:sl18e14@ecs.soton.ac.uk; meh@ecs.soton.ac.uk; lh@ecs.soton.ac.uk).

The research data supporting the paper can be obtained from the University of Southampton institutional repository: 10.5258/SOTON/D1000.

TABLE I
CONTRASTING OF THE CONTRIBUTIONS

Contributions	⋆	[6]-2015	[14]-2016	[11]-2018	[12]-2018	[17]-2018	[18]-2019
Separate multi-dimensional indexing	✓						✓
CS precoding at the transmitter	✓			✓	✓		✓
Symbol-level transmit antenna activation	✓	✓					
Large-scale MIMO	✓	✓					
Multi-user scenarios	✓	✓					
ABEP Analysis	✓	✓					✓
CS based reduced-complexity multi-user detector	✓						
Imperfect CSI	✓			✓			
Soft optimal multi-user detector	✓						
Soft reduced-complexity multi-user detector	✓						
Maximum achievable rate analysis based on EXIT charts	✓				✓		✓

information. Hence Hamming codes [20], convolutional codes (CC) [21], turbo codes [22] as well as diverse other channel coding techniques [23] have been proposed as promising FEC coding techniques since the 1950s. As a further advance, extrinsic information transfer (EXIT) charts were introduced in [24] and [25], which is a powerful semi-analytical tool for analysing the convergence behaviour of iterative systems and for evaluating their achievable throughput (Tp). The authors of [26] and [27] have explored the bit-interleaved coded modulation (BICM) which is one of the coded modulation schemes [28] eminently suitable for MU-MIMO systems, where the performance gain compared to the uncoded scenario was substantiated by numerical results.

In this paper, we propose both uncoded and coded CS-aided two-dimensional IM for the LS-MU-MIMO-UL combining the benefits of LS-MU-MIMO, SM, GSM, OFDM-IM and CS for UL transmission over frequency-selective fading channels. We refer to the proposed system as CS-aided generalised space-frequency IM (CS-GSFIM) designed for the LS-MU-MIMO-UL, emphasising that this is the first contribution exploring the multi-dimensional IM technique in large-scale multi-user scenarios. Specifically, we contrast our contributions in Table I to the most relevant treatises cited in our paper. In our proposed design, we index the TAs and the subcarriers separately for attaining higher design flexibility than the joint space-frequency indexing strategy of [14], [17]. Additionally, in order to increase the diversity gain attained as well as to improve the performance, flexibly selectable different TA activation patterns are employed for different transmitted symbols instead of using the same active TAs for the entire subcarrier group, as in [18]. Then a reduced-complexity MUD is designed for striking an attractive bit error rate (BER) vs complexity trade-off, where the design of the reduced-complexity MUD makes our CS-GSFIM scheme an attractive choice for LS-MU-MIMO communications.

Against the above background, the contributions of this paper are summarised as follows:

- A CS-GSFIM scheme is proposed for LS-MU scenarios in order to strike a better performance vs complexity trade-off than the conventional LS-MU-MIMO-OFDM systems. This is the first contribution exploring the multi-dimensional IM technique in LS-MU scenarios. The basic idea of the proposed CS-GSFIM scheme is that for each user, the information is conveyed by three parts, namely by the frequency-domain (FD) IM, the spatial-domain (SD) IM and by the classic APM symbols. Additionally, a more flexible index activation strategy is conceived for the proposed CS-GSFIM system than the joint space-frequency activation patterns of [14]. Explicitly, we propose independent TA activation patterns and subcarrier activations for further improving the flexibility of the system's design. More particularly, in order to attain an improved diversity gain, in contrast to the multi-dimensional scheme of [18], different TA activation patterns may be employed for the different transmitted APM symbols instead of fixing the active TAs for the entire OFDM subcarrier group.
- We then analyse the average bit error probability (ABEP) of the proposed CS-GSFIM system using ML detection and we derive an upper bound of the ABEP. Our numerical results demonstrate that the proposed MU CS-GSFIM scheme is capable of achieving better BER performance than both the conventional MU-MIMO-OFDM scheme, as well as the MU multi-dimensional IM scheme relying on the same TA activation pattern for each subcarrier group of [18] and the MU CS-aided frequency-domain IM of [11], at the same SE.
- Then our reduced search-space based iterative matching pursuit (RSS-IMP) detector is proposed for the CS-GSFIM system, which relies on sophisticated CS principles. The computational complexities are compared for the proposed systems using both the ML detector, as well as the minimum mean square error (MMSE) detector and the RSS-IMP detector. We demonstrate that the RSS-IMP detector is capable of striking a better BER performance vs complexity trade-off than both the conventional MU-MIMO-OFDM system using the ML detector and the proposed systems using the MMSE detector, despite its significantly reduced complexity. This makes the proposed CS-GSFIM system eminently suitable for LS-MU-MIMO communications.
- We then proceed by investigating the performances of the proposed CS-GSFIM scheme in the presence of imperfect channel state information (ICSI). It is demonstrated by our simulation results that our scheme is more robust to channel estimation errors than the conventional MU-MIMO-OFDM system.
- For the sake of attaining a near-capacity performance, we then design specific soft MUDs based on both the ML detector and on the RSS-IMP detector which rely on

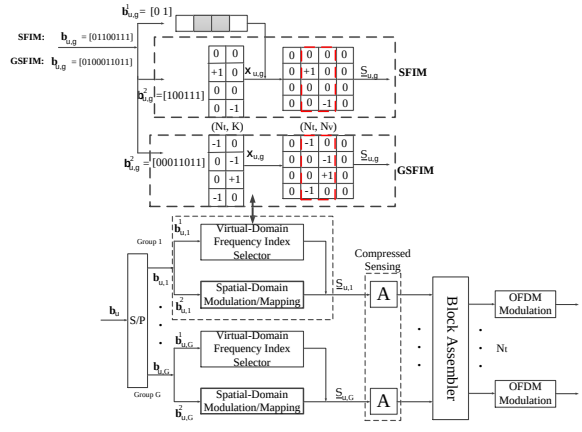

Fig. 2. The transmitter architecture of the novel CS-GSFIM scheme of Fig. 1 at the user terminal.

iteratively exchanging soft information with the FEC decoders. Our FEC-coding based numerical results indicate that near-capacity performances can indeed be achieved by the proposed MUDs. Additionally, we investigate the maximum achievable rates of the proposed CS-GSFIM system by appropriately configuring the system parameters with the aid of EXIT charts.

The remainder of this paper is organised as follows. Section II introduces the UL transmission process of the proposed system and Section III describes both the ML multi-user detector as well as the RSS-IMP multi-user detector designed for both hard-decision (HD) and soft-decision (SD) detection. Additionally, the average complexity orders of the different multi-user detectors are provided in Section III-C. In Section IV, our simulation results are presented, including both the uncoded and coded BER performances as well as the capacity analysis. Finally, the paper is concluded in Section V.

II. System Model

In this section, we introduce the proposed LS-MU CS-GSFIM architecture supporting U UL users, as shown in Fig. 1, where each user is equipped with N_t TAs for simultaneously communicating with a BS having N_r RAs, where N_r is on the order of tens to hundreds. The transmitter of our CS-GSFIM scheme at the user terminal is illustrated in Fig. 2, where both CS-aided frequency-domain IM and spatial-domain IM techniques are designed for each user in order to improve the UL Tp vs EE. The specific procedures of the proposed CS-GSFIM system are detailed in the following subsections.

A. Uplink Transmission

In the block diagram of the proposed LS-MU CS-GSFIM system seen in Fig. 1, there are U UL users communicating with a BS and the novel CS-GSFIM-OFDM technique is exploited for each user. As shown in Fig. 2, the information sequence $\mathbf{b_u}$[1] of the u-th UL user is split into G subcarrier groups [7] for implementing the CS-GSFIM-OFDM technique, where all the G subcarrier groups have the same process as seen in Fig. 2, but the frequency index selection, the TA selection and the transmitted APM symbols may vary among the different subcarrier groups. As shown in Fig. 2, in the g-th subcarrier group of the u-th user, the information sequence $\mathbf{b}_{u,g}$ is split into $\mathbf{b}^1_{u,g}$ and $\mathbf{b}^2_{u,g}$, which are conveyed by Virtual-Domain Frequency Index Selector block and the Spatial-Domain Modulation/Mapping block, respectively.

1) Virtual-Domain Frequency Index Selector: The bit sequence $\mathbf{b}^1_{u,g}$ of length $\lfloor \log_2(C^K_{N_v}) \rfloor$ is forwarded to the Virtual-Domain Frequency Index Selector of Fig. 2. For each subcarrier block, only K active subcarriers are selected out of the N_v available subcarriers by the Virtual-Domain Frequency Index Selector of Fig. 2, and the specific selection procedure is determined by the incoming bits $\mathbf{b}^1_{u,g}$, where a look-up table example is provided in Table II for $K = 2$ and $N_v = 4$. Explicitly, if $\mathbf{b}^1_{u,g} = [0\,0]$, then the first and the second subcarriers are activated for transmitting symbols. More explicitly, as shown in Fig. 2, the Virtual-Domain Frequency Index Selector is illustrated based on the look-up table example of Table II, where the incoming information sequence is assumed to be $\mathbf{b}^1_{u,g} = [0\,1]$, while the second and the third subcarriers, which are shaded in Fig. 2, are activated accordingly.

2) Spatial-Domain Modulation/Mapping: For each subcarrier group, the information sequence $\mathbf{b}^2_{u,g}$ is fed into the SD Modulation/Mapping block of Fig. 2. In this section, both the SM/Mapping having $N^a_t = 1$ and the GSM/Mapping having $1 < N^a_t \leq N_t$ are explicitly explained as follows.

a) SM/Mapping ($N^a_t = 1$): In a given channel use of the SM scheme, the information bits are divided into two parts, where $\lfloor \log_2 C(N_t, 1) \rfloor$ bits are used for activating one out of N_t TAs and $\log_2 \mathcal{L}$ bits are mapped to an $\mathcal{L}$-ary classic APM symbol. In the architecture illustrated in Fig. 2, we have K active subcarriers in each subcarrier group, which indicates that the Spatial-Domain Modulation/Mapping block

[1]For an uncoded scenario, the information sequence $\mathbf{b_u}$ represents the source information, and for the coded scenario, $\mathbf{b_u}$ represents the RSC coded information sequence.

TABLE II
A Look-up Table Example of CS-IM for $K = 2$ and $N_v = 4$.

Input Bits	Activated Indices	Allocation
$[0\,0]$	$\{1, 2\}$	$[K_1\, K_2\, \mathbf{0}\, \mathbf{0}]$
$[0\,1]$	$\{2, 3\}$	$[\mathbf{0}\, K_1\, K_2\, \mathbf{0}]$
$[1\,0]$	$\{3, 4\}$	$[\mathbf{0}\, \mathbf{0}\, K_1\, K_2]$
$[1\,1]$	$\{1, 4\}$	$[K_1\, \mathbf{0}\, \mathbf{0}\, K_2]$

TABLE III
A look-up table example of SM/Mapping for $N_t = 4$, $N^a_t = 1$, $\mathcal{L} = 2$ and $K = 2$.

Input Bits	Antenna Indices	APM Symbols	Allocations
$[000000]$	$1; 1$	$-1, -1$	$[-1\,0\,0\,0]$; $[-1\,0\,0\,0]$
$[010001]$	$1; 2$	$-1, +1$	$[-1\,0\,0\,0]$; $[0\,+1\,0\,0]$
$[100111]$	$2; 4$	$+1, -1$	$[0\,+1\,0\,0]$; $[0\,0\,0\,-1]$
$[110100]$	$2; 1$	$+1, +1$	$[0\,+1\,0\,0]$; $[+1\,0\,0\,0]$
$[001000]$	$3; 1$	$-1, -1$	$[0\,0\,-1\,0]$; $[-1\,0\,0\,0]$
$[011011]$	$3; 4$	$-1, +1$	$[0\,0\,-1\,0]$; $[0\,0\,0\,+1]$
$[101100]$	$4; 1$	$+1, -1$	$[0\,0\,0\,+1]$; $[-1\,0\,0\,0]$
$[111110]$	$4; 3$	$+1, +1$	$[0\,0\,0\,+1]$; $[0\,0\,+1\,0]$

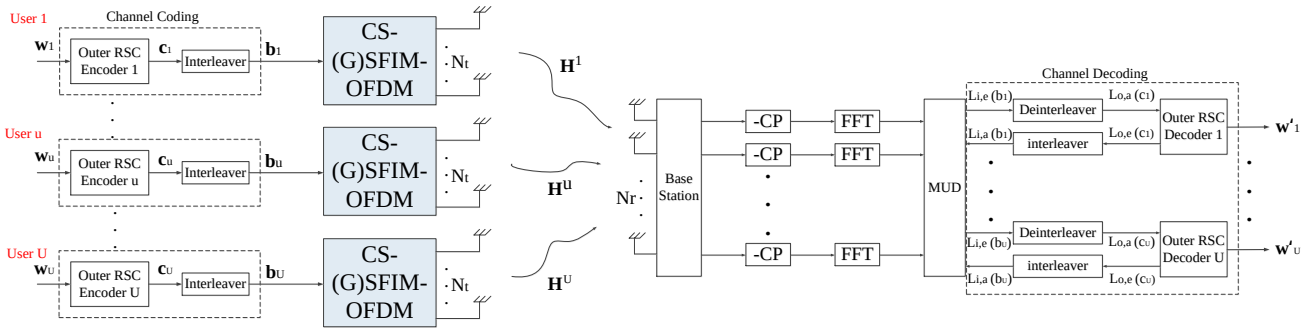

Fig. 1. The coded CS-GSFIM system's transceiver architecture, where the BS is equipped with N_r RAs to serve the U UL users and each user is equipped with N_t TAs.

of Fig. 2 maps K $\mathcal{L}$-ary APM symbols in each subcarrier block to the corresponding active TAs for transmission. Hence, the information sequence $\mathbf{b}^2_{u,g}$ in the g-th subcarrier block of the u-th user has the length of $(K\log_2\mathcal{L} + K\lfloor\log_2 C(N_t,1)\rfloor)$ bits, which combines both $(K\log_2\mathcal{L})$ bits for modulating K $\mathcal{L}$-ary APM symbols and $K\lfloor\log_2 C(N_t,1)\rfloor$ bits for selecting the active TAs in order to transmit K APM symbols. As shown in Table III[2], we apply $K = 2$ activated BPSK symbols and each BPSK symbol will be transmitted through $N_t^a = 1$ active TA out of $N_t = 4$ available TAs, where $(K\log_2\mathcal{L}+K\lfloor\log_2 C(N_t,1)\rfloor) = (2\times\log_2 2+2\times\lfloor\log_2 4\rfloor) = 6$ bits are mapped to each subcarrier block. More explicitly, if $\mathbf{b}^2_{u,g} = [100111]$, then both the second and the fourth TAs are activated for transmitting the BPSK symbol $(+1)$ and the BPSK symbol (-1), respectively, whilst resulting in the allocation blocks $[0+1\,0\,0]$ and $[0\,0\,0-1]$, as seen in Table III. Specifically, in contrast to the indexing strategy of the literature [18] applying the same active TAs combination for symbols in the same subcarrier group, the Spatial-Domain Modulation of Fig. 2 is capable of carrying more information bits. Following the process of SM/Mapping, the signal matrix $\mathbf{X}_{u,g} \in \mathbb{C}^{N_t\times K}$ is obtained, which is also illustrated in Fig. 2.

b) GSM/Mapping ($1 < N_t^a \leq N_t$): In order to further increase the BE of the proposed system, GSM is utilised in the architecture seen in Fig. 2, where $1 < N_t^a \leq N_t$ out of N_t TAs are activated in our scenario. Explicitly, the information sequence $\mathbf{b}^2_{u,g}$ in the g-th subcarrier block of the u-th user has the length of $(N_t^a K\log_2\mathcal{L} + K\lfloor\log_2 C(N_t,N_t^a)\rfloor)$ bits, which combines both $(N_t^a K\log_2\mathcal{L})$ bits for modulating $(N_t^a\cdot K)$ $\mathcal{L}$-ary APM symbols and $K\lfloor\log_2 C(N_t,N_t^a)\rfloor$ bits for selecting multiple active TAs for different symbols. Assuming that we have $K = 2, N_t^a = 2, N_t = 4$ and $\mathcal{L} = 2$, the information sequence $\mathbf{b}^2_{u,g}$ has the length of $(2\times 2\log_2 2 + 2\times\lfloor\log_2 C(4,2)\rfloor) = 8$ bits. More explicitly, if the incoming information sequence is $\mathbf{b}^2_{u,g} = [00011011]$, as seen in the example illustrated in Fig. 2, then the first and fourth TAs are activated for transmitting the BPSK symbols (-1) and (-1), while the second and third TAs are activated for transmitting the BPSK symbols (-1) and $(+1)$, when having $K = 2$. Compared to the information sequence associated with $N_t^a = 1$, more information can be transmitted due to the increased number of active TAs.

3) Space-Frequency Index Modulation: According to the specific active subcarrier selection regime of the VD frequency index selector introduced in Section II-A1 and the output matrix $\mathbf{X}_{u,g} \in \mathbb{C}^{N_t\times K}$ of the SD modulation/mapping illustrated in Section II-A2, the space-frequency matrix $\underline{\mathcal{S}}_{u,g} \in \mathbb{C}^{N_t\times N_v}$ is obtained by allocating the column vectors of the SD matrix $\mathbf{X}_{u,g}$ to the selected active subcarriers. In general, the space-frequency matrix $\underline{\mathcal{S}}_{u,g}$ for each subcarrier block has a sparsity level of $N_t^a\cdot K$, where there are K active subcarriers per space-frequency block and there are N_t^a active TAs for transmitting the signals at each active subcarrier, which results in $N_t^a\cdot K$ non-zero elements in the space-frequency matrix $\underline{\mathcal{S}}_{u,g}$.

4) Compressed Sensing and the Block Assembler: There are G space-frequency matrices $\underline{\mathcal{S}}_{u,g}$ $(g = 1,2,\ldots G)$ for the u-th user, where G represents the number of subcarrier blocks per OFDM frame. For each subcarrier block of the u-th user, a CS measurement matrix $\mathbf{A} \in \mathbb{C}^{m\times N_v}$ is employed for compressing the N_v-dimensional vector $\underline{\mathcal{S}}^t_{u,g}$ from the t-th TA in the VD into an m-dimensional vector $\mathbf{s}^t_{u,g}$ from the t-th TA in the FD, which can be expressed as

$$\mathbf{s}^t_{u,g} = \mathbf{A}\underline{\mathcal{S}}^t_{u,g}, \tag{1}$$

where $t = 1,2,\ldots,N_t$ and we can express the FD signals arriving from the N_t TAs in the g-th subcarrier block of the u-th user as $\mathbf{S}_{u,g} \in \mathbb{C}^{N_t\times m}$. Then, the Block Assembler collects G FD signals $\mathbf{S}_{u,g}$ to create a space-frequency super frame $\mathbf{S}_u \in \mathbb{C}^{N_t\times N_c}$, which contains N_t OFDM symbols for transmission from N_t TAs and can be expanded as $\mathbf{S}_u = [\mathbf{S}_{u,1},\mathbf{S}_{u,2},\ldots,\mathbf{S}_{u,G}]$. Afterwards, inverse Fast Fourier transform (IFFT) is applied to the OFDM symbol at each TA for obtaining the time-domain (TD) symbol, followed by concatenating the usual cyclic prefix (CP). Then, as shown in Fig. 1, the resultant TD signals of the u-th user are simultaneously transmitted from the N_t TAs over the wireless channel.

Considering the UL transmission of U users, the generalised system's overall achievable rate (bits/s/Hz) based on the above discussions is expressed as [11]

$$R_t = U\cdot\frac{G(N_t^a K\log_2 L + K\lfloor\log_2(C^{N_t^a}_{N_t^a})\rfloor + \lfloor\log_2 C^K_{N_v}\rfloor)}{N_c + N_{cp}}. \tag{2}$$

[2]There are 64 combinations in total and we use 8 out of the total combinations as an example in Table III.

III. Multi-user Detection

Let $\mathbf{H}^u \in \mathbb{C}^{N_r \times N_t}$ $(u = 1, 2, \ldots, U)$ denote the MIMO channel matrix of the u-th user, where $\mathbf{H}_i^u[n] \in \mathbb{C}^{1 \times N_t}$ $(i = 1, 2, \ldots, N_r$ and $n = 1, 2, \ldots, N_c)$ denotes the complex channel gain of the n-th subcarrier spanning from the N_t TAs of the u-th user to the i-th RA. Assuming perfect synchronisation, the signal $\mathbf{y}_i^u[n]$ received from the u-th user at the i-th RA after the CP removal and FFT-based demodulation is given by

$$\mathbf{y}_i^u[n] = \mathbf{H}_i^u[n]\mathbf{S}_u[n] + \mathbf{w}_i^u[n], \tag{3}$$

where $n = 1, 2, \ldots, N_c$ denotes the index of the transmitted FD subcarriers of the u-th user, $\mathbf{S}_u[n] \in \mathbb{C}^{N_t \times 1}$ denotes the FD symbols received at the n-th subcarrier from the N_t TAs and $\mathbf{w}_i^u[n]$ is the Gaussian noise with zero mean and variance of σ^2.

After collecting the received FD symbols $\mathbf{y}_i^u[n]$ $(n = 1, 2, \ldots, N_c)$ at the N_c subcarriers, we can express the signal $\mathbf{y}_i^u \in \mathbb{C}^{N_c \times 1}$ received by the i-th RA from the u-th user as

$$\mathbf{y}_i^u = \mathbf{H}_i^u \mathbf{s}_u + \mathbf{w}_i^u, \tag{4}$$

where $\mathbf{H}_i^u \in \mathbb{C}^{N_c \times (N_t N_c)} = diag\{\mathbf{H}_i^u[n]\}$ $(n = 1, 2, \ldots, N_c)$ denotes the diagonal-structure of the complex-valued channel gain matrix for the transmission of N_c FD subcarriers of the u-th user from the N_t TAs to the i-th RA, $\mathbf{s}_u \in \mathbb{C}^{(N_t N_c) \times 1} = [(\mathbf{S}_u[1])^T (\mathbf{S}_u[2])^T \ldots (\mathbf{S}_u[N_c])^T]^T$ represents the N_c-length FD symbols of the u-th user transmitted from the N_t TAs, while having $(N_t^a \cdot K \cdot G)$ non-zero elements, and $\mathbf{w}_i^u \in \mathbb{C}^{N_c \times 1}$ denotes the Gaussian noise vector, which obeys the distribution of $\mathcal{CN}(0, \sigma^2)$.

When all users simultaneously transmit their own signals from the N_t TAs, the FD signal $\mathbf{y}_i \in \mathbb{C}^{N_c \times 1}$ received at the i-th RA is expressed as

$$\mathbf{y}_i = \sum_{u=1}^{U} \mathbf{y}_i^u = \mathbf{H}_i \mathbf{s} + \mathbf{w}_i, \tag{5}$$

where $\mathbf{H}_i = [\mathbf{H}_i^1 \mathbf{H}_i^2 \ldots \mathbf{H}_i^U]$, $\mathbf{s} \in \mathbb{C}^{(N_t N_c U) \times 1} = [(\mathbf{s}_1)^T (\mathbf{s}_2)^T \ldots (\mathbf{s}_U)^T]^T$, and $\mathbf{w}_i$ is the Gaussian noise matrix.

Stacking the received signal $\mathbf{y}_i$ in (5) over the N_r RAs at the BS, we can express the received signal $\mathbf{y} \in \mathbb{C}^{(N_r N_c) \times 1}$ as

$$\mathbf{y} = \mathbf{H}\mathbf{s} + \mathbf{w}, \tag{6}$$

where $\mathbf{y} = [\mathbf{y}_1^T \mathbf{y}_2^T \ldots \mathbf{y}_{N_r}^T]^T$, $\mathbf{H} \in \mathbb{C}^{(N_r N_c) \times (N_t N_c U)} = [\mathbf{H}_1^T \mathbf{H}_2^T \ldots \mathbf{H}_{N_r}^T]^T$ and $\mathbf{w} \in \mathbb{C}^{(N_r N_c) \times 1} = [\mathbf{w}_1^T \mathbf{w}_2^T \ldots \mathbf{w}_{N_r}^T]^T$.

For the sake of analysis, the FD received signal $\mathbf{y}$ in (6) can be split into G subcarrier groups and the signal $\mathbf{y}_g \in \mathbb{C}^{(N_r m) \times 1}$ of the g-th subcarrier group of the U users received from the N_t TAs over the N_r RAs at the BS can be represented by

$$\mathbf{y}_g = \mathbf{H}_g \mathbf{s}_g + \mathbf{w}_g, \tag{7}$$

where $\mathbf{s}_g \in \mathbb{C}^{(N_t m U) \times 1}$ denotes the signals transmitted to the U users of the g-th subcarrier group from the N_t TAs and $\mathbf{w}_g \in \mathbb{C}^{N_r m \times 1}$ is the Gaussian noise vector. The equivalent channel matrix $\mathbf{H}_g \in \mathbb{C}^{(N_r m) \times (N_t m U)}$ associated with transmitting the signals of U users in the g-th subcarrier group from the N_t TAs over the N_r RAs can be expanded as

$$\mathbf{H}_g = \begin{bmatrix} \mathbf{H}_{1,g}^1 & \mathbf{H}_{1,g}^2 & \cdots & \mathbf{H}_{1,g}^U \\ \mathbf{H}_{2,g}^1 & \mathbf{H}_{2,g}^2 & \cdots & \mathbf{H}_{2,g}^U \\ \vdots & \vdots & \ddots & \vdots \\ \mathbf{H}_{N_r,g}^1 & \mathbf{H}_{N_r,g}^2 & \cdots & \mathbf{H}_{N_r,g}^U \end{bmatrix}, \tag{8}$$

where the element matrix $\mathbf{H}_{i,g}^u \in \mathbb{C}^{m \times (N_t m)}$ in (8) represents the complex channel at the i-th RA of the u-th user received from the N_t TAs, which can be written as

$$\mathbf{H}_{i,g}^u = \begin{bmatrix} \mathbf{H}_{i,g}^u[1] & \mathbf{0} & \cdots & \mathbf{0} \\ \mathbf{0} & \mathbf{H}_{i,g}^u[2] & \cdots & \mathbf{0} \\ \vdots & \vdots & \ddots & \vdots \\ \mathbf{0} & \mathbf{0} & \cdots & \mathbf{H}_{i,g}^u[m] \end{bmatrix}. \tag{9}$$

In (9), we use $\mathbf{H}_{i,g}^u[n] \in \mathbb{C}^{1 \times N_t}$ $(n = 1, 2, \ldots, m)$ to represent the complex channel gain for the n-th FD subcarrier in the g-th subcarrier group of the u-th user spanning from the N_t TAs to the i-th RA.

Explicitly, based on the process of the proposed CS-GSFIM-OFDM in Fig. 2, the signals $\mathbf{s}_g$ in (7) transmitted to the g-th group can be expressed as

$$\mathbf{s}_g = \bar{\mathbf{A}} \mathbf{I}_{SI}^g \mathbf{I}_{AC}^g \mathbf{x}_L^g, \tag{10}$$

where $\bar{\mathbf{A}} \in \mathbb{C}^{(N_t m U) \times (N_t N_v U)}$ denotes the group-equivalent[3] CS measurement matrix of $\mathbf{A}$ in (1), $\mathbf{I}_{SI}^g \in \mathbb{C}^{(N_t N_v U) \times (N_t K U)}$ is the group-equivalent representation of the subcarrier indexing pattern, $\mathbf{I}_{AC}^g \in \mathbb{C}^{(N_t K U) \times (K N_t^a U)}$ represents the group-equivalent TA indexing for U users in the g-th subcarrier group and we have the generalised expression of (10), since $1 \leq N_t^a \leq N_t$. Furthermore, $\mathbf{x}_L^g \in \mathbb{C}^{K N_t^a U \times 1}$ in (10) indicates the vector containing $K N_t^a U$ transmitted APM symbols in the g-th subcarrier group for U users, where we have $1 \leq N_t^a \leq N_t$. Then (7) can be written as

$$\mathbf{y}_g = \mathbf{H}_g \bar{\mathbf{A}} \mathbf{I}_{SI}^g \mathbf{I}_{AC}^g \mathbf{x}_L^g + \mathbf{w}_g = \mathbf{H}_g \bar{\mathbf{A}} \mathbf{I}_g \mathbf{x}_L^g + \mathbf{w}_g, \tag{11}$$

where $\mathbf{I}_g \in \mathbb{C}^{(N_t N_v U) \times (K N_t^a U)} = \mathbf{I}_{SI}^g \mathbf{I}_{AC}^g$ is the equivalent supporting matrix containing the information of the active TAs and the active subcarriers of U users in the g-th subcarrier group.

In the following, we will detail both the hard-decision (HD) based ML detector and the soft-decision (SD) based ML, which are then followed by the portrayal of both the HD and SD based reduced-complexity RSS-IMP detectors.

A. Maximum Likelihood Multi-User Detector

In this section, we introduce both the HD-aided and the SD-aided ML detectors proposed for the uncoded and coded CS-GSFIM system, respectively.

- *HD-aided ML Detector*: For the uncoded scenario of the proposed system illustrated in Fig. 1, information

[3]We use a large-dimension matrix $\bar{\mathbf{A}}$ derived from $\mathbf{A}$ to represent the measurement matrix for compressing signals of U users transmitted from N_t TAs, where we call this large-dimension matrix "group-equivalent" matrix.

sequences $\mathbf{w}_u$ $(u = 1, 2, \ldots, U)$ at the transmitter is processed directly on a group-by-group basis by the CS-GSFIM-OFDM encoder shown in Fig. 1 and Fig. 2. Then, the signal received at the BS is detected by our MUD of Fig. 1. Note that for the sake of simplicity, we only introduce the HD-aided ML algorithm for the g-th subcarrier group here, which can be generalised to the entire OFDM symbol.

Let us assume that $< l_g, i_g, j_g >$ corresponds to the specific input information in the g-th subcarrier group for U users of the proposed system shown in Fig. 1. Explicitly, $(\mathbf{x}_L^g)_{l_g}$ denotes the l_g-th realisation of the KN_t^aU APM symbols for $l_g = 1, 2, \ldots, L^{KN_t^aU}$, $(\mathbf{I}_{SI}^g)_{i_g}$ represents the i_g-th indexing pattern of the active subcarriers of the U users, given that $i_g = 1, 2, \ldots, N_{SI}^U$, and $(\mathbf{I}_{AC}^g)_{j_g}$ is used to denote the j_g-th active TAs selection pattern for KU active subcarriers of U users in the g-th subcarrier group for $j_g = 1, 2, \ldots, (N_{AC}^K)^U$. Additionally, we use $< \hat{l}_g, \hat{i}_g, \hat{j}_g >$ to represent the estimate of the corresponding input information. Then the HD-aided optimal ML detector of (6) and (11) is expressed as

$$\begin{aligned} &< \hat{l}_g, \hat{i}_g, \hat{j}_g > \\ &= \arg \min_{l_g, i_g, j_g} \|\mathbf{y}_g - \mathbf{H}_g \bar{\mathbf{A}} (\mathbf{I}_{SI}^g)_{i_g} (\mathbf{I}_{AC}^g)_{j_g} (\mathbf{x}_L^g)_{l_g}\|^2 \\ &= \arg \min_{l_g, i_g, j_g} \|\mathbf{y}_g - \mathbf{H}_g \bar{\mathbf{A}} \bar{\mathbf{s}}_g\|^2, \end{aligned} \tag{12}$$

where we use $\bar{\mathbf{s}}_g = (\mathbf{I}_{SI}^g)_{i_g} (\mathbf{I}_{AC}^g)_{j_g} (\mathbf{X}_L^g)_{l_g}$ to denote the search space of the g-th subcarrier group and the ML detector achieves the optimal detection performance in uncoded scenarios.

- *Average BEP*: Here, we derive the ABEP of the proposed multi-user scenario using ML detection for a single subcarrier group, since all subcarrier groups have the same pairwise error (PE) event. Considering the system model of the g-th subcarrier group given in (7), if $\mathbf{S}_g$ is transmitted but erroneously detected as $\hat{\mathbf{s}}_g \in \mathbb{C}^{(N_t mU) \times 1}$, given the channel matrix $\mathbf{H}_g$ in the FD, then the conditional pairwise error probability (CPEP) is expressed as [29]

$$P(\mathbf{s}_g \to \hat{\mathbf{s}}_g | \mathbf{H}_g) = Q\left(\sqrt{\frac{\|\mathbf{H}_g(\mathbf{s}_g - \hat{\mathbf{s}}_g)\|^2}{2\sigma^2}}\right). \tag{13}$$

Then (13) can be rewritten by using the alternative form of the Q-function as

$$P(\mathbf{s}_g \to \hat{\mathbf{s}}_g | \mathbf{H}_g) = \frac{1}{\pi} \int_0^{\pi/2} \exp\left(-\frac{\xi_d}{4\sigma^2 \sin^2\theta}\right) d\theta, \tag{14}$$

where we define

$$\xi_d = \|\mathbf{H}_g(\mathbf{s}_g - \hat{\mathbf{s}}_g)\|^2 \tag{15}$$

$$= \sum_{j=1}^{mU} \|\mathbf{H}_g^j(\mathbf{s}_g^j - \hat{\mathbf{s}}_g^j)\|^2 \tag{16}$$

$$= \sum_{j=1}^{mU} \sum_{i=1}^{N_r} (\mathbf{H}_g^j)_i (\mathbf{s}_g^j - \hat{\mathbf{s}}_g^j)(\mathbf{s}_g^j - \hat{\mathbf{s}}_g^j)^H (\mathbf{H}_g^j)_i^H, \tag{17}$$

and $(\mathbf{H}_g^j)_i \in \mathbb{C}^{1 \times N_t}$ is the i-th row element of $\mathbf{H}_g^j \in \mathbb{C}^{N_r \times N_t}$. Then the moment generating function (MGF) [30] of ξ_d defined in (15) can be obtained according to the quadratic form of ξ_d provided in (17) as

$$M_{\xi_d}(t) = \prod_{j=1}^{mU} \frac{1}{\left(1 - t\|\mathbf{s}_g^j - \hat{\mathbf{s}}_g^j\|^2\right)^{N_r}}. \tag{18}$$

Finally, integrating the CPEP given in (14) over the probability density function of ξ_d and using the MGF $M_{\xi_d}(t)$ given in (18), the unconditional pairwise error probability (UPEP) is obtained as

$$P(\mathbf{s}_g \to \hat{\mathbf{s}}_g) = \frac{1}{\pi} \int_0^{\pi/2} \prod_{j=1}^{mU} \left(\frac{\sin^2\theta}{\sin^2\theta + \frac{\|\mathbf{s}_g^j - \hat{\mathbf{s}}_g^j\|^2}{4\sigma^2}}\right)^{N_r} d\theta. \tag{19}$$

After obtaining the UPEP in (19), an upper bound of the ABEP based on the union bound can be obtained by [29]

$$P_B \leq \frac{1}{bN(\mathbf{s}_g)} \sum_{\mathbf{s}_g} \sum_{\hat{\mathbf{s}}_g} P(\mathbf{s}_g \to \hat{\mathbf{s}}_g) d\left[P(\mathbf{s}_g, \hat{\mathbf{s}}_g)\right], \tag{20}$$

where b is the number of information bits transmitted by the U users in the UL within each subcarrier group, $N(\mathbf{s}_g)$ is the total number of legitimate realisations of $\mathbf{s}_g$ for U users per subcarrier group and $d\left[P(\mathbf{s}_g, \hat{\mathbf{s}}_g)\right]$ is used for representing the number of erroneous bits for the PE event of $(\mathbf{s}_g \to \hat{\mathbf{s}}_g)$.

- *SD-aided Detector*: Having presented the HD-aided ML detector of the CS-GSFIM system, we present the SD-aided iterative detection technique based on the classic Logarithmic Maximum *a posteriori* (Log-MAP) algorithm [31]. As illustrated in Fig. 1, there are U two-stage serially concatenated systems, which incorporate the MUD and U half-rate RSC decoders. The MUD and each RSC decoder are connected by an interleaver and deinterleaver pair, as shown in Fig. 1. Specifically, the received complex-valued signal $\mathbf{y}$ in (6) is demapped by the MUD shown in Fig. 1 to its log likelihood ratio (LLR) representations for the channel-coded bits of each of the U users. The MUD's extrinsic output LLRs $L_{M,e}$ of the u-th user are deinterleaved by the soft-bit deinterleaver of Fig. 1 for generating the *a priori* LLRs $L_{R,a}$ entered into the RSC decoder in order to calculate the extrinsic LLRs $L_{R,e}$ based on the Log-MAP algorithm [31] for all channel-coded symbols of the u-th user. As seen in Fig. 1, $L_{R,e}$ is then appropriately reordered as $L_{M,a}$ by the soft-bit interleaver and fed back to the MUD as the *a priori*

information for providing improved extrinsic LLRs. The improved extrinsic LLRs are then passed to the RSC decoder and then back to the MUD for further inner-outer (IO) iterations.

Using the received signal model of (6), the conditional probability of receiving the signal $\mathbf{y}$ given the full search-space $\bar{\mathbf{s}}$ while exploring all realisations of the CS-GSFIM for U users can be expressed as

$$p(\mathbf{y}|\bar{\mathbf{s}}) = \frac{1}{(\pi N_0)^{N_r U}} \exp\left(-\frac{\|\mathbf{y} - \mathbf{H}\bar{\mathbf{s}}\|^2}{N_0}\right). \quad (21)$$

According to the UL transmission of the U users discussed in Section II-A, the received signal $\mathbf{y}$ of (6) carries $\mathbf{b} = [\mathbf{b}_1\, \mathbf{b}_2\, \ldots\, \mathbf{b}_u\, \ldots\, \mathbf{b}_U]$ channel-coded bits, as seen in Fig. 1, where each user carries B channel coded bits and we use $b_u(i)$ $(i = 1, 2, \ldots, B)$ to represent the u-th user's channel-coded bits. Then the extrinsic LLR value of $b_u(i) \in \mathbf{b}_u$ can be expressed as

$$\begin{aligned} L_{M,e}\left[b_u(i)\right] &= \ln\left(\frac{p(b_u(i)=1|\mathbf{y})}{p(b_u(i)=0|\mathbf{y})}\right) \\ &= \ln\left(\frac{\sum_{\bar{\mathbf{s}}\in\bar{\mathbf{s}}_1^{b_u(i)}} \exp\left(\Phi_{l,i,j}\right)}{\sum_{\bar{\mathbf{s}}\in\bar{\mathbf{s}}_0^{b_u(i)}} \exp\left(\Phi_{l,i,j}\right)}\right), \end{aligned} \quad (22)$$

where $\bar{\mathbf{s}}_1^{b_u(i)}$ and $\bar{\mathbf{s}}_0^{b_u(i)}$ are the subsets of $\bar{\mathbf{s}}$ satisfying $\bar{\mathbf{s}}_1^{b_u(i)} \triangleq \{\bar{\mathbf{s}}_{l,i,j} \in \bar{\mathbf{s}} : b_u(i) = 1\}$ and $\bar{\mathbf{s}}_0^{b_u(i)} \triangleq \{\bar{\mathbf{s}}_{l,i,j} \in \bar{\mathbf{s}} : b_u(i) = 0\}$, respectively. Additionally, the *a posteriori* symbol probability $\Phi_{l,i,j}$ in (22) is expressed by

$$\Phi_{l,i,j} \triangleq -\frac{\|\mathbf{y} - \mathbf{H}\bar{\mathbf{s}}\|^2}{N_0} + \sum_{j\neq i} b_u(j) L_{M,a}\left[b_u(j)\right]. \quad (23)$$

In order to avoid numerical overflow, the Jacobian logarithm of [31] is applied for simplifying the SD-aided detection of (22) as

$$L_{M,e}\left[b_u(i)\right] = \text{jac}_{\bar{\mathbf{s}}\in\bar{\mathbf{s}}_1^{b_u(i)}}(\Phi_{l,i,j}) - \text{jac}_{\bar{\mathbf{s}}\in\bar{\mathbf{s}}_0^{b_u(i)}}(\Phi_{l,i,j}). \quad (24)$$

B. RSS-IMP Multi-User Detector

The ML detector introduced in Section III-A achieves the optimal detection performance due to the full search-space detection, where all possible combinations of the APM symbols, the active TAs and the active subcarriers of all users are explored. However, the detection complexity of the ML detector discussed in Section III-A may become excessive in practice, for example in our LS-MU-MIMO scenarios. Hence, we propose an RSS-IMP multi-user detector in this section, which iteratively reduces the detector's search space and splits the detection process into several sub-operations with the aid of CS principles. We introduce the reduced-complexity detector in this section based on the received group-equivalent signal $\mathbf{y}_g$ in (7) and (11), which contains all information in the g-th subcarrier group from all users, where we can re-express (11) as

$$\mathbf{y}_g = \bar{\mathbf{H}}_g \bar{\mathbf{s}}_g + \mathbf{w}_g, \quad (25)$$

where $\bar{\mathbf{H}}_g \in \mathbb{C}^{(N_r m)\times(N_t N_v U)} = \mathbf{H}_g \bar{\mathbf{A}}$ is the equivalent channel matrix of all users in the g-th subcarrier group and $\bar{\mathbf{s}}_g \in \mathbb{C}^{(N_t N_v U)\times 1}$ is the transmitted group-equivalent signal covering all the U users' information received from the active TAs, the active subcarriers and the APM symbols.

Specifically, in the CS-GSFIM scheme illustrated in Fig. 2, the transmitted group-equivalent signal $\bar{\mathbf{s}}_g$ has an intrinsic sparsity level of $(KN_t^a U)$, where only $KN_t^a U$ elements in $\bar{\mathbf{s}}_g$ are non-zero. Additionally, (25) reveals its over-determined nature (*e.g.* having $N_r m > N_t N_v U$) due to the large number of RAs at the BS and hence the CS-based sparse detection algorithm [32] can be applied to the detector according to CS principles [33].

In (25), the group-equivalent channel matrix $\bar{\mathbf{H}}_g$ fulfils the mutual incoherence property (MIP) [33] requirement for guaranteeing a good detection performance according to CS principles, so that $\bar{\mathbf{H}}_g$ can be regarded as a group-equivalent measurement matrix in our following discussions and $\bar{\mathbf{s}}_g$ is a sparse signal, which will be detected with the aid of CS.

Based on the classic greedy algorithm's philosophy and on the iterative algorithm of [32], the proposed RSS-IMP detector searches through multiple promising candidates during each iteration and the number of promising candidates increases with the number of iterations. Then the proposed RSS-IMP detector makes a decision concerning the best candidate at the end of the process. More specifically, the proposed RSS-IMP detector intrinsically amalgamates the classic greedy algorithm and the iterative algorithm for tackling the detection challenge of the proposed CS-GSFIM system operating in LS-MU-MIMO scenarios. Explicitly, the proposed RSS-IMP detector is composed of three steps, namely the application of conventional linear detection for initially generating rough estimates and mitigating the MU interference, followed by the iterative detection technique of [32] and the final decision based on minimising the residual error vector, as detailed in the following.

- Step 1:
  The linear minimum mean square error (LMMSE) detector is applied to the received signal $\mathbf{y}_g$ of (25) both for mitigating the MU interference, and for generating a rough estimate $\hat{\mathbf{s}}_g \in \mathbb{C}^{(N_t N_v U)\times 1}$ of the transmitted sparse signal $\bar{\mathbf{s}}_g$ of (25), which can be expressed as

  $$\hat{\mathbf{s}}_g = \left(\bar{\mathbf{H}}_g^H \bar{\mathbf{H}}_g + \frac{1}{\gamma}\mathbf{I}_{(N_t N_v U)}\right)^{-1} \bar{\mathbf{H}}_g^H \mathbf{y}_g, \quad (26)$$

  where $\hat{\mathbf{s}}_g$ is the estimated signal of the g-th subcarrier group of the U users, containing the information of the active TAs, of the active subcarriers and of the APM symbols. Furthermore, $\gamma = E\|\bar{\mathbf{H}}_g \bar{\mathbf{s}}_g\|_2^2 / E\|\mathbf{w}_g\|_2^2$ is the average SNR per symbol. Additionally, the estimated signal $\hat{\mathbf{s}}_g$ can be split into U vectors in parallel, which can be reformulated as a matrix $\left[\hat{\mathbf{s}}_g^1 \ldots \hat{\mathbf{s}}_g^u \ldots \hat{\mathbf{s}}_g^U\right]^T$ of size $(U \times N_t N_v)$, where $\hat{\mathbf{s}}_g^u \in \mathbb{C}^{N_t N_v \times 1}$ $(u = 1, 2, \ldots, U)$ is the LMMSE estimated signal of the u-th user. There should be KN_t^a active elements in $\hat{\mathbf{s}}_g^u$. According to the index separation strategy illustrated in (10) and (11), the estimated signal $\hat{\mathbf{s}}_g^u$ for the u-th user can be expressed as

  $$\hat{\mathbf{s}}_g^u = \mathbf{I}_g^u \mathbf{x}_L^{g,u} + \hat{\mathbf{w}}_g^u, \quad (27)$$

where $\mathbf{I}_g^u \in \mathbb{C}^{N_t N_v \times K N_t^a} = \mathbf{I}_{SI}^{g,u} \mathbf{I}_{AC}^{g,u}$ represents the joint support matrix containing the activation patterns of the active TAs $\mathbf{I}_{AC}^{g,u} \in \mathbb{C}^{N_t N_v \times N_t K}$ and the active subcarriers $\mathbf{I}_{SI}^{g,u} \in \mathbb{C}^{N_t K \times K N_t^a}$ for the u-th user in the g-th subcarrier group, $\mathbf{x}_L^{g,u} \in \mathbb{C}^{K N_t^a \times 1}$ represents the APM symbols vector of the u-th user and finally $\hat{\mathbf{w}}_g^u \in \mathbb{C}^{N_t N_v \times 1}$ is the linear-processed Gaussian noise vector.

Then we calculate the magnitudes of $(N_t N_v)$ elements in $\hat{\mathbf{s}}_g^u$ and rearrange these magnitudes in a descending order, where the ordered magnitudes of the U users can be expressed as

$$\left[\begin{array}{c} \|\hat{\mathbf{s}}_g^1(i_1^1)\|^2 > \|\hat{\mathbf{s}}_g^1(i_2^1)\|^2 > \cdots > \|\hat{\mathbf{s}}_g^1(i_{N_t N_v}^1)\|^2 \\ \vdots \\ \|\hat{\mathbf{s}}_g^u(i_1^u)\|^2 > \|\hat{\mathbf{s}}_g^u(i_2^u)\|^2 > \cdots > \|\hat{\mathbf{s}}_g^u(i_{N_t N_v}^u)\|^2 \\ \vdots \\ \underbrace{\|\hat{\mathbf{s}}_g^U(i_1^U)\|^2}_{1^{st}Iteration} > \underbrace{\|\hat{\mathbf{s}}_g^U(i_2^U)\|^2}_{2^{nd}Iteration} > \underbrace{\cdots}_{\cdots} > \underbrace{\|\hat{\mathbf{s}}_g^U(i_{N_t N_v}^U)\|^2}_{(N_t N_v)^{th}Iteration} \end{array}\right], \tag{28}$$

where for example, $\|\hat{\mathbf{s}}_g^u(i_1^u)\|^2$ is the highest magnitude of the u-th user and hence the i_1^u-th element $\hat{\mathbf{s}}_g^u(i_1^u)$ in $\hat{\mathbf{s}}_g^u$ has the highest probability to be one of the KN_t^a active elements. In addition, we use N^u to indicate the total number of joint realisations[4] in each subcarrier group of the u-th user, while selecting KN_t^a active elements out of $(N_t N_v)$ transmitted elements, where we have $N^u = N_{SI} N_{AC}^K$. Explicitly, a set of realisations Z_u^1 of the u-th user is selected during the 1^{st} iteration and we have $Z_u^1 < N^u$, where the resultant sets of realisations $\left[Z_1^1\ Z_2^1\ \ldots\ Z_U^1\right]$ of the U users during the 1^{st} iteration will be employed in the second step.

- Step 2:
  In the second step, we carry out the proposed iterative detection based on the greedy algorithm for detecting both the indices of the active TAs, as well as the indices of the active subcarriers and the corresponding APM symbols of all users.

  During the first iteration of the u-th user, there are Z_u^1 realisations of the joint-support matrix $\mathbf{I}_g^u$ in (27) and we refer to these Z_u^1 realisations as the joint-support matrix candidates in the first iteration of the u-th user. Then the joint-support matrix candidates in the first iteration derived for the u-th user are expressed as

$$\{\mathbf{I}_g^u\}_1 = \{\mathbf{I}_{g,1}^u, \mathbf{I}_{g,2}^u, \cdots, \mathbf{I}_{g,Z_u^1}^u\}. \tag{29}$$

  Specifically, based on the estimated signal of (27), we can obtain the estimated signal $\hat{\mathbf{y}}_g^u \in \mathbb{C}^{N_r m \times 1}$ received from the u-th user, which is expressed as

$$\hat{\mathbf{y}}_g^u = \mathbf{\Omega}_g^u \mathbf{x}_L^{g,u} + \hat{\bar{\mathbf{w}}}_g^u, \tag{30}$$

  where we define $\mathbf{\Omega}_g^u \in \mathbb{C}^{(N_r m) \times (K N_t^a)} = \mathbf{H}_g^u \bar{\mathbf{A}}^u \mathbf{I}_g^u$ as a group-equivalent matrix, while $\hat{\bar{\mathbf{w}}}_g^u \in \mathbb{C}^{N_r m \times 1}$ represents the Gaussian noise vector. According to the candidate set generated during the first iteration listed in (29), the Z_u^1 group-equivalent matrix candidates in the first iteration can be represented as $\{\mathbf{\Omega}_{g,1}^u, \mathbf{\Omega}_{g,2}^u, \cdots, \mathbf{\Omega}_{g,Z_u^1}^u\}$. Additionally, the system of (30) is referred to as an over-determined scenario, since $N_r m > K N_t^a$ and hence the pseudo-inverse process can be exploited for detecting the transmitted signals. Then the pseudo-inverse process of the i-th group-equivalent matrix candidate $\mathbf{\Omega}_{g,i}^u$ $(i = 1, 2, \ldots, Z_u^1)$ is expressed as

$$(\mathbf{\Omega}_{g,i}^u)^\dagger = \left(\left(\mathbf{\Omega}_{g,i}^u\right)^H \mathbf{\Omega}_{g,i}^u\right)^{-1} \left(\mathbf{\Omega}_{g,i}^u\right)^H. \tag{31}$$

  Upon substituting (31) into (30), the estimated signal $\hat{\mathbf{x}}_{L,i}^{g,u} \in \mathbb{C}^{K N_t^a \times 1}$ is obtained as

$$\begin{aligned} \hat{\mathbf{x}}_{L,i}^{g,u} &= (\mathbf{\Omega}_{g,i}^u)^\dagger (\mathbf{\Omega}_g^u \mathbf{x}_L^{g,u} + \hat{\bar{\mathbf{w}}}_g^u) \\ &= \mathbf{x}_L^{g,u} + \bar{\mathbf{w}}_g^u + \mathbf{r}_{g,i}^u, \end{aligned} \tag{32}$$

  where the linearly processed Gaussian noise vector $\bar{\mathbf{w}}_g^u$ still remains Gaussian distributed, and $\mathbf{r}_{g,i}^u$ is the residual error vector due to the mismatch[5] of the matrix candidate $\mathbf{\Omega}_{g,i}^u$ and the correct matrix $\mathbf{\Omega}_g^u$.

  Then the symbol-by-symbol optimal ML algorithm is applied to the estimated $\hat{\mathbf{x}}_{L,i}^{g,u}$ in (32) for detecting the APM symbols based on the i-th tested CS matrix candidate $\mathbf{\Omega}_{g,i}^u$ during the first iteration and this process is represented as

$$\vec{\mathcal{X}}_{L,i}^{g,u}(n) = \arg\min_{\mathcal{A}} \|\hat{\mathbf{x}}_{L,i}^{g,u}(n) - \mathcal{A}_L\|^2, \tag{33}$$

  where $n = 1, 2, \ldots, K N_t^a$, $\mathcal{A}_L \in \mathcal{A}$ represents the library of L-ary APM symbols and $\vec{\mathcal{X}}_{L,i}^{g,u}(n)$ is the n-th estimated APM symbol.

  Then we have the group-equivalent matrix candidate $\mathbf{\Omega}_{g,i}^u$, the corresponding estimated symbols vector $\vec{\mathcal{X}}_{L,i}^{g,u}$, and the received signal $\hat{\mathbf{y}}_g^u$ in (30). Now we can calculate the residual error value $\mathcal{R}_{g,i}^u$ by testing the i-th matrix candidate during the first iteration, yielding

$$\mathcal{R}_{g,i}^u = \|\hat{\mathbf{y}}_g^u - \mathbf{\Omega}_{g,i}^u \vec{\mathcal{X}}_{L,i}^{g,u}\|^2. \tag{34}$$

  Additionally, Z_u^1 residual error values $\{\mathcal{R}_{g,1}^u, \mathcal{R}_{g,2}^u, \cdots, \mathcal{R}_{g,i}^u, \cdots, \mathcal{R}_{g,Z_u^1}^u\}$ are collected during the first iteration and the specific candidate resulting in the minimum residual error is the output of the first iteration, yielding

$$\mathbf{\Omega}_{g,best}^u|_1 = \arg\min_{Z_u^1} \{\mathcal{R}_{g,i}^u\}, \tag{35}$$

  where $\mathbf{\Omega}_{g,best}^u|_1$ is the most reliable group-equivalent matrix candidate giving the minimum residual error $\{\mathcal{R}_{g,min}^u\}_1$ during the first iteration.

  Then the same process is repeated for the further iterations according to the ordered magnitudes shown in (28).
- Step 3:
  During the third step, we make the final decision concerning the best candidate by comparing the minimal residual errors $\{\mathcal{R}_{g,min}^u\}$ from the different iterations, where for

[4]Note that each realisation is a joint combination of the active TAs and the active subcarriers per subcarrier group for the u-th user, and we have $N^u < C_{N_t N_v}^{K N_t^a}$ due to the index separation strategy imposed at the transmitter.

[5]If the testing candidate $\mathbf{\Omega}_{g,i}^u = \mathbf{\Omega}_g^u$, the residual error vector $\mathbf{r}_{g,i}^u$ should be all zeros.

example, if the minimal residual error during the first iteration $\{\mathcal{R}^u_{g,min}\}_1$ is the minimum value among the different iterations, then the best candidate matrix of the u-th user is determined as $\mathbf{\Omega}^u_{g,best}|_1$.

Additionally, in order to implement the SD-aided detection presented in Section III-A, the extrinsic LLRs are calculated using the so-called Approx-Log-MAP algorithm formulated in (24). Based on the received signal model of the g-th subcarrier group in (30) and the UL transmission of U users presented in Section II-A, the received signal $\mathbf{y}_g$ carries $\mathbf{b}_g = [\mathbf{b}_{1,g}\, \mathbf{b}_{2,g}\, \ldots\, \mathbf{b}_{u,g}\, \ldots \mathbf{b}_{U,g}]$ $(u = 1, 2, \ldots, U)$ channel-coded bits, where each user carries $\frac{B}{G}$ channel-coded bits and $b_{u,g}(i)$ $(i = 1, 2, \ldots, \frac{B}{G})$ denotes the channel coded bits of the u-th user in the g-th subcarrier group. Specifically, the extrinsic LLR value of $b_{u,g}(i) \in \mathbf{b}_g$ is expressed by

$$L_{M,e}\left(b_{u,g}(i)\right) = \text{jac}_{n^\alpha \in n^\alpha_{b_{u,g}(i)=1}}\{d\} - \text{jac}_{n^\alpha \in n^\alpha_{b_{u,g}(i)=0}}\{d\}, \tag{36}$$

where $n^\alpha_{b_{u,g}(i)=1}$ and $n^\alpha_{b_{u,g}(i)=0}$ denote the index of the CS matrix candidate during the α-th iteration for $\mathbf{\Omega}^u_g$ and $\mathbf{x}^{g,u}_L$ of (30), when the i-th bit is fixed to 1 and 0, respectively. Furthermore, d in (36) denotes the *a posteriori* symbol probability, which is represented as

$$d = -\frac{\|\hat{\mathbf{y}}^u_g - \mathbf{\Omega}^u_{g,n^\alpha}\vec{\mathcal{X}}^{g,u}_{L,n^\alpha}\|^2}{N_0} + \sum_{j\neq i} b_{u,g}(j) L_{M,a}\left[b_{u,g}(j)\right]. \tag{37}$$

C. Computational Complexity

In this subsection, the complexity orders of the ML, MMSE and the RSS-IMP detectors are analysed based on the size of their search space. As discussed in Section II, for every subcarrier group of each user, we have N_{FI} possible active subcarrier index combinations, N^K_{AC} possible active TA index realisations and $L^{K\cdot N^a_t}$ possible classical APM symbols combinations.

- *ML Detector:*
  In terms of the detection model $\|\mathbf{y}_g - \mathbf{H}_g\bar{\mathbf{A}}(\mathbf{I}^g_{SI})_{i_g}(\mathbf{I}^g_{AC})_{j_g}(\mathbf{x}^g_L)_{l_g}\|^2$ of (12), the detector will have a complexity order of $\mathcal{O}_{ML}\left[(N_{FI}N^K_{AC}L^{K\cdot N^a_t})^U\right]$, which may be excessive.
- *MMSE Detector:*
  The MMSE detector is presented as a bench-marker of the proposed RSS-IMP detector based on the operation of $\left(\mathbf{H}^H_g\mathbf{H}_g + \frac{1}{\gamma}\mathbf{I}\right)^{-1}\mathbf{H}^H_g\mathbf{y}_g$, where the complexity order is $\mathcal{O}_{MMSE}\left[U\cdot(N_{FI}N^K_{AC}L^{K\cdot N^a_t})\right]$.
- *RSS-IMP Detector:*
  According to the introduction of the proposed RSS-IMP detector of Section III-B, the computational complexity of the RSS-IMP detector mainly depends on the number of iterations applied. The complexity of the proposed RSS-IMP detector associated with detecting U users in terms of the search space can be expressed as

$$\mathcal{O}_{RSS-IMP}\left[L\cdot N^a_t\cdot K(N_1+N_2+\cdots+N_i)\right], \tag{38}$$

  where i $(1 \leq i \leq N_v)$ represents the iteration index and N_i indicates the number of joint realisations, including the active TAs and the active subcarriers of U users during the i-th iteration.

TABLE IV
COMPARISON OF AVERAGE COMPLEXITY ORDERS

N^a_t	Average complexity orders of the ML detector, the MMSE detector and the RSS-IMP detector for detecting all users of the CS-GSFIM system having $U = 12, N_t = 4, N_r = 64, N_c = 128, N_{cp} = 8, N_v = 16, m = 8, K = 2$, 8QAM			
	bits/s/Hz/user	ML $\mathcal{O}(\cdot)$	MMSE $\mathcal{O}(\cdot)$	RSS-IMP (All Iters) $\mathcal{O}(\cdot)$
1	1.88	$(6.6\times10^4)^{12}$	7.86×10^5	1.96×10^5
2	2.59	$(4.2\times10^6)^{12}$	5.03×10^7	3.93×10^5
3	3.29	$(2.7\times10^8)^{12}$	4.03×10^8	5.88×10^5
4	3.53	$(1.1\times10^9)^{12}$	2.01×10^8	4.92×10^5

In Table IV, the average complexity orders of the ML, the MMSE and of the RSS-IMP detector associated with detecting all users of the CS-GSFIM scheme proposed for LS-MU-MIMO are compared upon varying the value of N^a_t, where the SE is improved upon increasing the values of N^a_t. Specifically, if $N^a_t = 1$, the system becomes the CS-SFIM and if $N^a_t > 1$, the system becomes the CS-GSFIM. More specifically, in the scenario of $N^a_t = N_t = 4$ shown in the table, the system becomes a special case of the CS-GSFIM, where all TAs are used for transmission and only FD IM is applied. We explore the full search[6] based operation of the RSS-IMP detector, which has the worst-case complexity and we have $(N_1 + N_2 + \cdots + N_i) = U\cdot N_{FI}\cdot N^K_{AC}$ in terms of (38). Note that we do not consider the complexity of the LMMSE operations in the MMSE detector and in the RSS-IMP detector of Table IV, since it is negligible compared to the excessive complexity of the ML detector. As seen from Table IV, the MMSE and the RSS-IMP detector impose much lower complexities. Specifically, the RSS-IMP detector is capable of significantly reducing the complexity compared to the MMSE detector. Additionally, the average complexity orders of the RSS-IMP detector increase more slowly with the improved SE instead of the exponential trend of the MMSE detector.

IV. Performance Results and Comparisons

In this section, we present our theoretical as well as simulation results characterising the proposed CS-GSFIM scheme in LS-MU-MIMO-UL scenarios using both the ML detector of Section III-A and the proposed RSS-IMP detector of Section III-B and compare them to the conventional MU-MIMO-OFDM systems, to the MU CS-aided frequency-domain IM schemes of [11] and to the MU CS-aided multi-dimensional IM schemes of [18]. Specifically, we also characterise the maximum achievable rate of the proposed system with the aid of EXIT charts. Furthermore, the coded BER performance of the proposed system is presented, demonstrating that a near-capacity performance is achieved. The simulation parameters are summarised in Table V.

TABLE V
SYSTEM PARAMETERS IN SIMULATIONS.

	N_c	N_{cp}	L-PSK/QAM	N_v	N_f	K	U	N_r	N_t	N_t^a
Scheme 1	128	8	4QAM	–	–	–	2	12	1	1
Scheme 2	128	8	BPSK	16	8	2	2	12	4	3
Scheme 3	128	8	BPSK	16	8	2	12	64	4	3
Scheme 4	128	8	BPSK	16	8	2	12	128	4	3
Scheme 5	128	8	4QAM	–	–	–	4	32	1	1
Scheme 6	128	8	8QAM	16	8	2	4	32	4	1
Scheme 7	128	8	BPSK	16	8	2	4	32	4	3
Scheme 8	128	8	BPSK	16	8	2	12	varying	4	3
Scheme 9	128	8	32QAM	16	8	2	2	12	1	1
Scheme 10	128	8	4QAM	16	8	2	2	12	4	2
Scheme 11	128	8	16QAM	20	8	2	3	36	8	1
Scheme 12	128	8	32QAM	24	8	2	3	36	8	1
Scheme 13	128	8	128QAM	20	8	2	3	36	1	1
Scheme 14	128	8	8QAM	16	8	2	2	12	4	1
Scheme 15	128	8	8QAM	16	8	2	2	12	4	2
Scheme 16	128	8	32QAM	16	8	4	2	12	4	1
Scheme 17	128	8	8QAM	16	8	2	12	64	4	1
Scheme 18	128	8	8QAM	16	8	2	12	64	4	2
Scheme 19	128	8	32QAM	16	8	4	12	64	4	1
Scheme 20	128	8	4QAM	–	–	–	12	varying	1	1

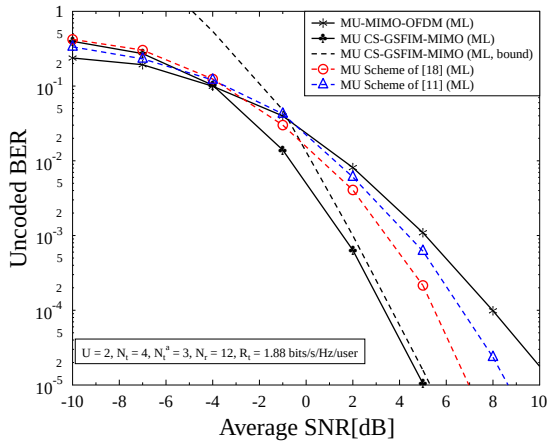

Fig. 3. Comparison between the uncoded BER performances of **Scheme 1**, **Scheme 2**, **Scheme 9** of [11] and **Scheme 10** of [18] shown in Table V using ML detectors, at the same rate of $R_t = 1.88$ bits/s/Hz/user.

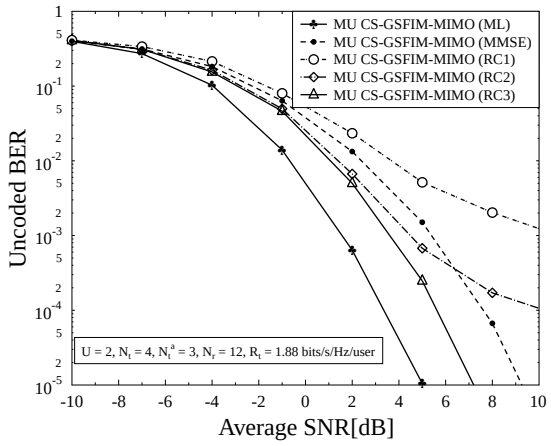

Fig. 4. Comparisons between uncoded BER performances of **Scheme 2** shown in Table V using both the MMSE detector and the proposed RSS-IMP MUD with $I = 1$ to 3 iterations applied, at the same rate of $R_t = 1.88$ bits/s/Hz/user.

A. Uncoded Performances

In Fig. 3, we compare the uncoded BER performances of **Scheme 1**, **Scheme 2**, **Scheme 9**[7] of [11] and **Scheme 10**[8] of [18], where the number of active TAs N_t^a is generalised, while supporting the same number of $U = 2$ users, employing the same number of $N_r = 12$ RAs and operating at the same rate of $R_t = 1.88$ bits/s/Hz/user. Observe in Fig. 3 that the MU CS-GSFIM-MIMO scheme using the ML detector outperforms the conventional MU-MIMO-OFDM scheme by about 5.5 dB at the BER value of 10^{-5} and at the same transmission rate. Specifically, the upper bound performance of the proposed system obtained by (20) is presented in Fig. 3, where it is observed that the upper bound is tight at moderate-to-high SNR values. Furthermore, **Scheme 2** of Table V attains about 2 dB and 3.5 dB SNR-gains over **Scheme 10** of [18] and **Scheme 9** of [11], respectively, again at the BER value of 10^{-5} and at the same transmission rate.

Additionally, in Fig 4, we portray the uncoded BER performances of the proposed scheme in conjunction with the parameters of **Scheme 2** using the reduced-complexity RSS-IMP MUD by using $I = 1$ to 3 iterations. More specifically, it is also shown in Fig 4 that the RSS-IMP MUD has the potential of approaching the optimal performance of the proposed generalised system using the ML detector. Observe

[6]"Full search" means that all possible joint realisations of active TAs and active subcarriers are explored, which is the worst-case complexity of the RSS-IMP detector and it is only used as a complexity bench-marker here. Indeed, it is unnecessary to explore full search in practice for achieving an attractive trade-off between the performance and the complexity order.

[7]**Scheme 9** is applied here to represent the CS-aided frequency-domain IM system and is a special instantiation of the scheme designed in [11].

[8]**Scheme 10** is a special instantiation of the CS-aided multi-dimensional IM scheme of [18], where the same activated distinctive TA combination is applied to each subcarrier group.

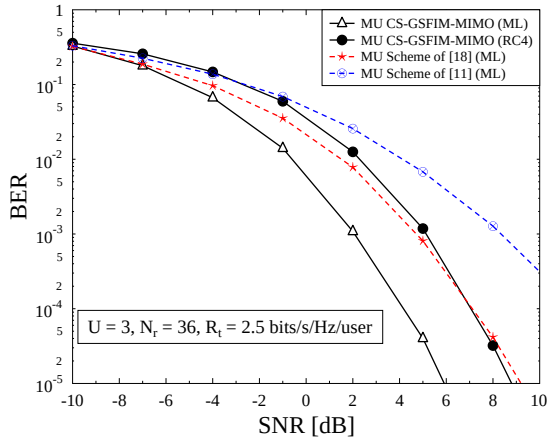

Fig. 5. Comparison between the uncoded BER performances of **Scheme 11** using both the ML detector and the proposed RSS-IMP detector, of **Scheme 12** using the ML detector and of **Scheme 13** using the ML detector, while supporting the same number of $U = 3$ users, the same number of RAs $N_r = 36$ and the same rate of $R_t = 2.5$ bits/s/Hz/user.

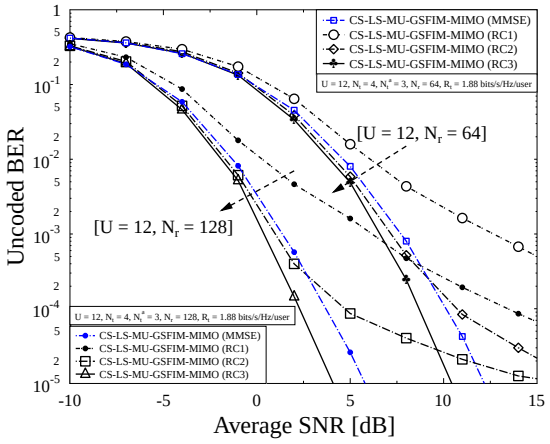

Fig. 6. Comparison between the uncoded BER performances of **Scheme 3** and **Scheme 4** for LS-MU-MIMO-UL scenario using both the MMSE detector and the proposed RSS-IMP detector having I = 1 to 3 iterations.

furthermore that the RSS-IMP MUD using only $I = 3$ iterations is capable of providing a better performance than the MMSE detector, even though the average complexity order $\mathcal{O}_{RSS-IMP}(8.2 \times 10^3)$ of the RSS-IMP detector using $I = 3$ iterations is much lower than the complexity $\mathcal{O}_{MMSE}(1.3 \times 10^5)$ of the MMSE detector.

In Fig. 5, we compare the uncoded BER performances of **Scheme 11**, **Scheme 12** of [18] and **Scheme 13** of [11] associated with the parameters listed in Table V at the same transmission rate of $R_t = 2.5$ bits/s/Hz/user. It is shown in Fig. 5 that the proposed CS-GSFIM scheme (**Scheme 11**) using the ML detector achieves about 3.2 dB SNR-gain over **Scheme 12** of [18] and outperforms **Scheme 13** of [11] about 9 dB at the BER value of 10^{-5} and at the same rate of 2.5 bits/s/Hz/user. Specifically, the RSS-IMP detector of **Scheme 11** associated with $I = 4$ iterations attains better performances than both **Scheme 12** of [18] and **Scheme 13** of [11] as well, at detection complexity order of $\mathcal{O}_{RSS-IMP}(6.9 \times 10^5)$, which is much lower than the $\mathcal{O}_{ML}(9.2 \times 10^{18})$ complexity of the ML detector.

Then in Fig. 6, we compare the uncoded BER performance of the RSS-IMP detector to that of the MMSE detector in conjunction with the parameters of ($N_c = 128$, $N_{cp} = 8$, $N_t = 4$, $N_t^a = 3$, $N_v = 16$, $m = 8$, $K = 2$, BPSK), where the MMSE detector is used as the benchmarker here and we have $U = 12$ UL users communicating with the aid of $N_r = 64$ RAs and $N_r = 128$ RAs, at the same SE of $R_t = 1.88$ bits/s/Hz/user. Note that the optimal ML detector of Section III-A has an excessive complexity for this LS-MU scenario. Hence, we are unable to show the performance of the ML detector in Fig. 6. It can be observed in Fig. 6 that the performance of the RSS-IMP detector is improved upon increasing the number of RAs due to the increased receive diversity order and only a few iterations are

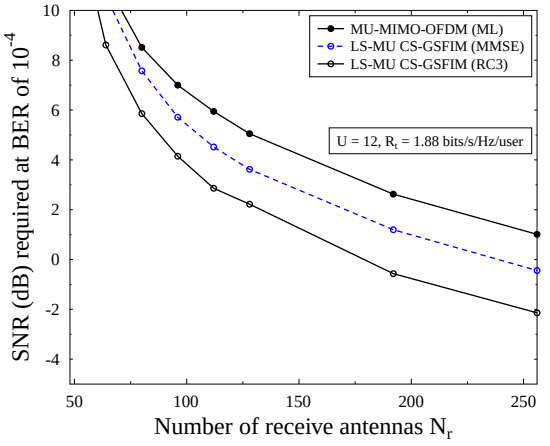

Fig. 7. Comparison of the SNRs required at the BER target of 10^{-4} with varying values of the RAs at the BS for **Scheme 8** using both the MMSE detector and the RSS-IMP detector using $I = 3$ iterations and for **Scheme 20** using the ML detector.

required for achieving a better performance than that of the MMSE detector. Explicitly, as shown in Table IV, we compare the complexity orders between the RSS-IMP detector using exhaustive full-search based iterations and the MMSE detector, where the RSS-IMP detector using exhaustive iterations has the best performance at the cost of the highest complexity order. Hence the RSS-IMP detector using I = 3 or 4 iterations presented in Fig. 6 has much lower complexity orders than that of the MMSE detector. It can be concluded that the RSS-IMP detector attains a near-optimal performance at a significantly lower complexity, which makes the proposed CS-GSFIM system attractive in LS-MU-MIMO scenarios.

In Fig. 7, we compare the SNRs required at the specific BER target of 10^{-4} for **Scheme 8** of Table V using both

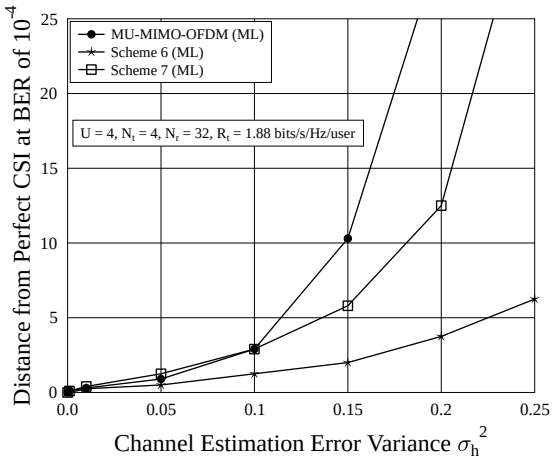

Fig. 8. SNR-penalty wrt the perfect CSI scenario at the BER target of 10^{-4}, where **Scheme 5**, **Scheme 6** and **Scheme 7** shown in Table V are employed and we have varying values of channel estimation error variance σ_h^2.

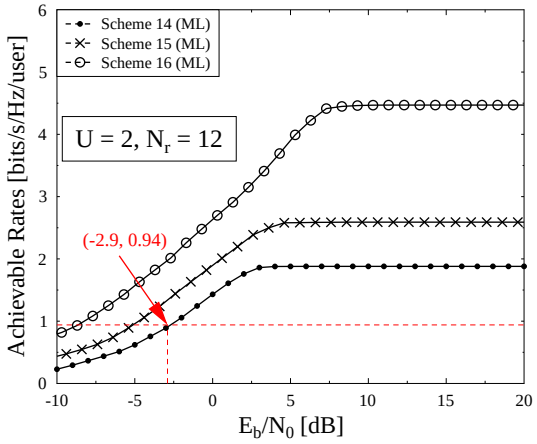

Fig. 9. Maximum achievable rates of **Scheme 14**, **Scheme 15** and **Scheme 16** in MU scenarios applying the ML detector.

the MMSE detector and the RSS-IMP detector employing $I = 3$ iterations, as well as for **Scheme 20** using the ML detector, while supporting the same number of $U = 12$ users, and the same rate of $R_t = 1.88$ bits/s/Hz/user as well as a varying number of RAs at the BS. Note that the optimal ML detector of Section III-A has an excessive complexity for this LS-MU scenario. Hence, we are unable to evaluate its performance in Fig. 7. Observe from Fig. 7 that the SNRs required by all these schemes are reduced upon increasing the number of RAs as a benefit of the improved receive diversity gain. Specifically, if the condition of $U \cdot N_t \geq N_r$ is satisfied, then the proposed system using the RSS-IMP detector becomes capable of outperforming both the classical MU-MIMO-OFDM system associated with the optimal ML detector and the proposed system using the MMSE detector.

In Fig. 8, the performances of the proposed systems in the presence of channel estimation errors are characterised, where the channel estimation errors at the receiver are assumed to obey the distribution of $\mathcal{CN}(0, \sigma_h^2)$ [34]. Three schemes (**Scheme 5**, **Scheme 6**, **Scheme 7**) are investigated in Fig. 8, while supporting the same number of $U = 4$ users, employing the same number of $N_r = 32$ RAs, at the same transmission rate of $R_t = 1.88$ bits/s/Hz/user and at varying values of channel estimation error variance δ_h^2. In Fig. 8, the SNR-distances between the SNR values of these three schemes having perfect CSI and the SNR values of these schemes relying on realistic imperfect CSI are compared at the specific target BER value of 10^{-4}. Observe from Fig. 8 that the proposed CS-GSFIM schemes (**Scheme 6** and **Scheme 7**) are more robust to channel estimation errors than the classical MU-MIMO-OFDM scheme (**Scheme 5**).

B. Maximum Achievable Rates

In Fig. 9 and Fig. 10, we analyse the achievable rates per user for different E_b/N_0 values of the CS-GSFIM in LS-MU-MIMO-UL scenarios in conjunction with different system

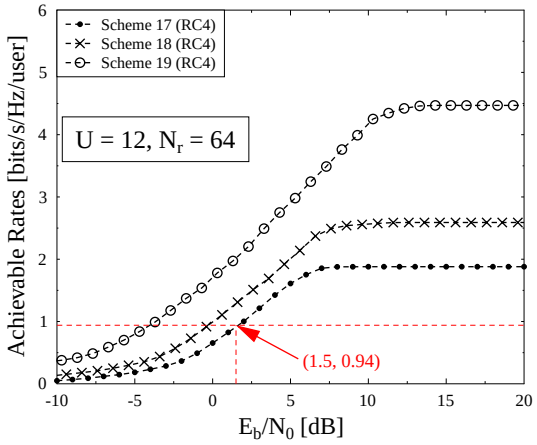

Fig. 10. Maximum achievable rates of **Scheme 17**, **Scheme 18** and **Scheme 19** in LS-MU scenarios applying the RSS-IMP detector using I = 4 iterations.

parameters by invoking the semi-analytical EXIT chart tool, where the maximum achievable rate of a system is equal to the area under the EXIT curve of the inner soft decoder [23], [35]. Explicitly, in Fig. 9 we portray the maximum achievable rate of **Scheme 14**, **Scheme 15** and **Scheme 16** of Table V applying the ML detector, while having $U = 2$ users and $N_r = 12$ RAs, as well as in Fig. 10 we portray the maximum achievable rate of **Scheme 17**, **Scheme 18** and **Scheme 19** of Table V applying the RSS-IMP detector associated with I = 4 iterations for efficiently reducing the complexity, while supporting $U = 12$ users and $N_r = 64$ RAs. Specifically, the proposed system's maximum achievable rate can be improved by increasing the number of active TAs N_t^a as well as by increasing the number of active subcarriers K or by increasing the size of APM symbol alphabet. It is also shown in Fig. 9 and Fig. 10 that the proposed generalised CS-GSFIM scheme is capable of

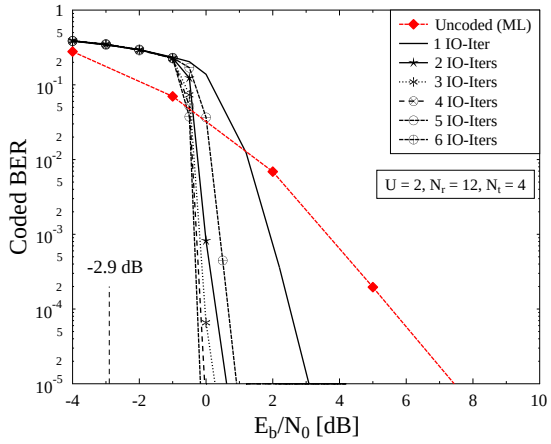

Fig. 11. The average BER performances of the iteratively detected half-rate RSC-coded system shown in Fig. 1 based on the detection of (24) in conjunction with the parameters of **Scheme 14** shown in Table V and an interleaver depth of $300,000$ bits while using $I_{IO} = 1$ to 4 iterations.

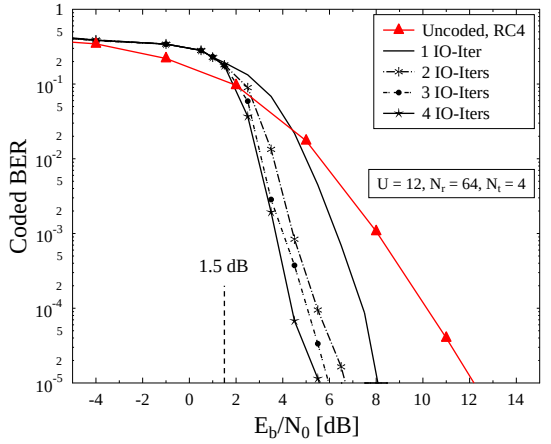

Fig. 12. The average BER performances of the iteratively detected half-rate RSC-coded system shown in Fig. 1 based on the detection of (36) using I = 4 iterations in conjunction with the parameters of **Scheme 17** shown in Table V and an interleaver depth of $300,000$ bits while using $I_{IO} = 1$ to 4 iterations.

achieving a higher rate than the CS-SFIM scheme advocated. In particular, when using a half-rate RSC channel encoder, the maximum achievable rate becomes 0.94 bits/s/Hz/user for both the proposed coded **Scheme 14** applying the ML detector and for the proposed **Scheme 17** applying the RSS-IMP detector (I = 4 iterations) at $E_b/N_0 = -2.9$ dB and $E_b/N_0 = 1.5$ dB, respectively, as indicated in Fig. 9 and Fig. 10.

C. Coded Performances

In Fig. 11 and Fig. 12, we characterise the BER performances of both the half-rate RSC-coded MU CS-GSFIM-MIMO scheme (**Scheme 14** of Table V) applying the ML detector and the half-rate RSC-coded LS-MU CS-GSFIM-MIMO scheme (**Scheme 17** of Table V) applying the reduced-

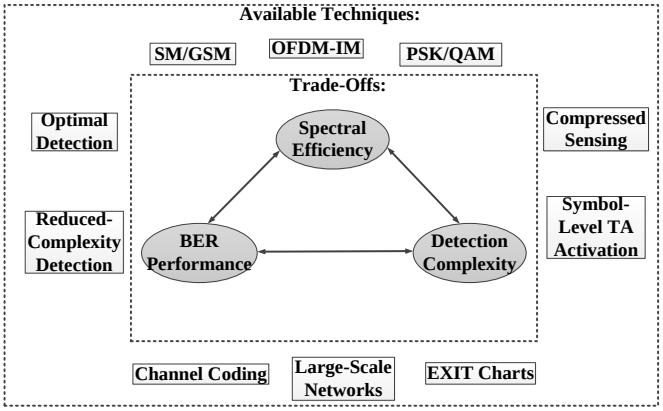

Fig. 13. Relationship of the diverse system components affecting the different design trade-offs.

complexity RSS-IMP detector ($I = 4$ iterations). An interleaver depth of $300,000$ bits is applied for each user, where $I_{IO} = 1$ to 6 inner-outer (IO) iterations and $I_{IO} = 1$ to 4 IO iterations are applied in **Scheme 14** using the ML detector and **Scheme 17** using the RSS-IMP detector, respectively. Observe in Fig. 11 and Fig. 12 that the coded BER performances approach the maximum achievable rate limits at both $E_b/N_0 = -2.9$ dB and $E_b/N_0 = 1.5$ dB with the aid of the IO iterative detection structure shown in Fig. 1. Explicitly, the performances of the coded systems approach the maximum achievable rate limit in Fig. 11 and Fig. 12 upon increasing the number of IO iterations, where the performances of the coded system ($I_{IO} = 6$ IO iterations) using the ML detector in Fig. 11 and of the coded system ($I_{IO} = 4$ IO iterations) using the reduced-complexity detector in Fig. 12 are about 2.8 dB and 4 dB away from the maximum achievable rate limits at the BER value of 10^{-5}, respectively. Specifically, in order to reduce the gap between the actually attained performance and the maximum achievable rate limit, the irregular convolutional codes (IrCCs) [36] aiming to match the specific shape of the EXIT curves of the inner and outer codes for reducing the 'open tunnel area' between them as discussed in [18] can be designed for encountering an open tunnel at the lowest possible E_b/N_0, where the distances of 2.8 dB and 4 dB shown in Fig. 11 and Fig. 12 will be significantly reduced.

V. Conclusions

A novel CS-GSFIM system with the index separation strategy for LS-MU-MIMO-UL communication has been proposed. Unlike the joint space-frequency indexing strategy in previous literature, the TAs and the subcarriers have been indexed separately for further improving the design flexibility. Additionally, in order to attain higher diversity gains, different TA activation patterns for different transmitted symbols have been employed instead of fixing the active TAs for the whole OFDM frame or for each subcarrier group. Due to the excessive complexity of the ML detector, a reduced-complexity RSS-IMP MUD based on both the classic greedy principle and iterative detection philosophy has been proposed, where the RSS-IMP MUD has struck an attractive BER performance vs

TABLE VI
SUMMARY OF SYSTEM TRADE-OFFS.

Scheme a	Scheme b	Rate (bits/s/Hz/user)	SNR (dB) gain at BER of 10^{-5} (a-b)	Complexity Ratio (a/b)
MU CS-GSFIM (ML)	MU Scheme of [18] (ML)	1.88	2	10^0
MU CS-GSFIM (ML)	MU Scheme of [11] (ML)	1.88	3.5	10^0
MU CS-GSFIM (ML)	MU CS-GSFIM (RC3)	1.88	2.05	5.2×10^5
MU CS-GSFIM (RC3)	MU CS-GSFIM (MMSE)	1.88	2.25	6.3×10^{-2}
MU CS-GSFIM (RC3)	MU Scheme of [18] (ML)	1.88	0.05	1.9×10^{-6}
MU CS-GSFIM (RC3)	MU Scheme of [11] (ML)	1.88	1.45	1.9×10^{-6}
MU CS-GSFIM (ML)	MU Scheme of [18] (ML)	2.5	3.2	10^0
MU CS-GSFIM (ML)	MU Scheme of [11] (ML)	2.5	9	10^0
MU CS-GSFIM (RC4)	MU CS-GSFIM (ML)	2.5	-2.8	8×10^{-14}
MU CS-GSFIM (RC4)	MU Scheme of [18] (ML)	2.5	0.4	7.5×10^{-14}
MU CS-GSFIM (RC4)	MU Scheme of [11] (ML)	2.5	6.2	7.5×10^{-14}
LS-MU CS-GSFIM (RC3)	LS-MU CS-GSFIM (MMSE)	1.88	2.1	1.1×10^{-1}

complexity trade-off. The low-complexity design of the RSS-IMP MUD has made the CS-GSFIM system an attractive one for LS-MU scenarios. Our simulation results characterising **Scheme 1**-**Scheme 20** of Table V have demonstrated that the performance of the RSS-IMP MUD using appropriate number of iterations in LS-MU scenarios outperforms both the classical MU-OFDM-MIMO system using the ML detector and the CS-GSFIM system using the MMSE detector at the same SE. Furthermore, the FEC-coded MUDs have been demonstrated to be capable of providing a near-capacity performance upon increasing the number of IO iterations. More specifically, we conclude that the proposed system strikes a flexible trade-off among the SE, BER and the complexity, which is an explicit benefit of the careful choice and configuration of the system components portrayed in Fig. 13. In order to elaborate further, we summarised the associated trade-offs in Table VI based on our simulation results of Fig. 3 - Fig. 6 at a glance. Observe that our MU scheme using the proposed RSS-IMP MUD associated with the most appropriate number of iterations is capable of approaching the optimal performance as well as of outperforming both the proposed MU scheme using the MMSE detector and the schemes of [11], [18] employed in MU scenarios, despite having a significantly lower complexity. Explicitly, it is promising to apply the proposed two-dimensional IM scheme in MU DL scenarios, where the joint design of the CS matrix and of the MU transmit precoder will be necessary for eliminating the MU interference and for guaranteeing an accurate recovery of the transmitted signals. Specifically, given the system components of Fig. 13, an adaptive MU scheme may be constructed by near-instantaneously re-configuring the different components of the scheme for maximising the system's achievable rate, while maintaining the target BER.

REFERENCES

[1] M. Jiang and L. Hanzo, "Multiuser MIMO-OFDM for next-generation wireless systems," *Proceedings of the IEEE*, vol. 95, no. 7, pp. 1430–1469, July 2007.

[2] S. Yang and L. Hanzo, "Fifty years of MIMO detection: the road to large-scale MIMOs," *IEEE Communications Surveys Tutorials*, vol. 17, no. 4, pp. 1941–1988, Fourthquarter 2015.

[3] R. Y. Mesleh, H. Haas, S. Sinanovic, C. W. Ahn, and S. Yun, "Spatial modulation," *IEEE Transactions on Vehicular Technology*, vol. 57, no. 4, pp. 2228–2241, July 2008.

[4] P. Yang, M. D. Renzo, Y. Xiao, S. Li, and L. Hanzo, "Design guidelines for spatial modulation," *IEEE Communications Surveys Tutorials*, vol. 17, no. 1, pp. 6–26, Firstquarter 2015.

[5] A. Younis, N. Serafimovski, R. Mesleh, and H. Haas, "Generalised spatial modulation," in *2010 Conference Record of the Forty Fourth Asilomar Conference on Signals, Systems and Computers*, Nov 2010, pp. 1498–1502.

[6] T. L. Narasimhan, P. Raviteja, and A. Chockalingam, "Generalized spatial modulation in large-scale multiuser MIMO systems," *IEEE Transactions on Wireless Communications*, vol. 14, no. 7, pp. 3764–3779, July 2015.

[7] E. Basar, U. Aygolu, E. Panayirci, and H. V. Poor, "Orthogonal frequency division multiplexing with index modulation," *IEEE Transactions on Signal Processing*, vol. 61, no. 22, pp. 5536–5549, Nov 2013.

[8] N. Ishikawa, S. Sugiura, and L. Hanzo, "50 years of permutation, spatial and index modulation: from classic RF to visible light communications and data storage," *IEEE Communications Surveys Tutorials*, vol. 20, no. 3, pp. 1905–1938, thirdquarter 2018.

[9] R. Fan, Y. J. Yu, and Y. L. Guan, "Generalization of orthogonal frequency division multiplexing with index modulation," *IEEE Transactions on Wireless Communications*, vol. 14, no. 10, pp. 5350–5359, Oct 2015.

[10] H. Zhang, L. L. Yang, and L. Hanzo, "Compressed sensing improves the performance of subcarrier index-modulation-assisted OFDM," *IEEE Access*, vol. 4, pp. 7859–7873, October 2016.

[11] S. Lu, I. A. Hemadeh, M. El-Hajjar, and L. Hanzo, "Compressed-sensing-aided space-time frequency index modulation," *IEEE Transactions on Vehicular Technology*, vol. 67, no. 7, pp. 6259–6271, July 2018.

[12] I. A. Hemadeh, S. Lu, M. El-Hajjar, and L. Hanzo, "Compressed sensing-aided index modulation improves space-time shift keying assisted millimeter-wave communications," *IEEE Access*, pp. 1–1, 2018.

[13] M. Yuzgecciogluu, E. Jorswieck, C. Theory, and C. Laboratory, "Uplink and downlink transceiver design for OFDM with index modulation in multi-user networks," in *2017 IEEE 28th Annual International Symposium on Personal, Indoor, and Mobile Radio Communications (PIMRC)*, Oct 2017, pp. 1–5.

[14] T. Datta, H. S. Eshwaraiah, and A. Chockalingam, "Generalized space-and-frequency index modulation," *IEEE Transactions on Vehicular Technology*, vol. 65, no. 7, pp. 4911–4924, July 2016.

[15] B. Shamasundar, S. Jacob, S. Bhat, and A. Chockalingam, "Multi-dimensional index modulation in wireless communications," in *2017 Information Theory and Applications Workshop (ITA)*, Feb 2017, pp. 1–10.

[16] P. Yang, Y. Xiao, Y. L. Guan, M. Di Renzo, S. Li, and L. Hanzo, "Multi-domain index modulation for vehicular communications: a survey," *IEEE Vehicular Technology Magazine*, 2018.

[17] R. Chen and J. Zheng, "Index-modulated MIMO-OFDM: joint space-frequency signal design and linear precoding in rapidly time-varying channels," *IEEE Transactions on Wireless Communications*, vol. 17, no. 10, pp. 7067–7079, Oct 2018.

[18] S. Lu, I. A. Hemadeh, M. El-Hajjar, and L. Hanzo, "Compressed sensing-aided multi-dimensional index modulation," *IEEE Transactions on Communications*, vol. 67, no. 6, pp. 4047–4087, June 2019.

[19] C. E. Shannon, "A mathematical theory of communication," *Bell Systems Technical Journal*, vol. 27, pp. 623–656, October 1948.

[20] R. W. Hamming, "Error detecting and error correcting codes," *Bell Systems Technical Journal*, vol. 29, pp. 41–56, 1950.

[21] P. Elias, "Coding for noisy channels," *IRE Conv. Rept.*, pp. 37–47, 1955.

[22] C. Berrou and A. Glavieux, "Near optimum error correcting coding and decoding: Turbo-codes," *IEEE Trans. Commun.*, vol. 44, no. 10, pp. 1261–1271, October 1996.

[23] L. Hanzo, T. H. Liew, B. L. Yeap, R. Y. S. Tee, and S. X. Ng, *Turbo coding, turbo equalisation and space-time coding:EXIT-chart-aided near-capacity designs for wireless channels*. Wiley-IEEE Press, 2011.

[24] S. ten Brink, "Convergence behavior of iteratively decoded parallel concatenated codes," *IEEE Transactions on Communications*, vol. 49, no. 10, pp. 1727–1737, Oct 2001.

[25] A. Ashikhmin, G. Kramer, and S. ten Brink, "Extrinsic information transfer functions: model and erasure channel properties," *IEEE Transactions on Information Theory*, vol. 50, no. 11, pp. 2657–2673, Nov 2004.

[26] L. He, J. Wang, and J. Song, "Multiuser detection for FEC-coded massive spatial modulation MIMO: an iterative interference rejection approach," *IEEE Transactions on Vehicular Technology*, vol. 66, no. 10, pp. 9567–9571, Oct 2017.

[27] J. Bao, Z. Ma, M. Xiao, T. A. Tsiftsis, and Z. Zhu, "Bit-interleaved coded SCMA with iterative multiuser detection: multidimensional constellations design," *IEEE Transactions on Communications*, pp. 1–1, 2017.

[28] G. Caire, G. Taricco, and E. Biglieri, "Bit-interleaved coded modulation," *IEEE Transactions on Information Theory*, vol. 44, no. 3, pp. 927–946, May 1998.

[29] M. D. Renzo and H. Haas, "Bit error probability of SM-MIMO over generalized fading channels," *IEEE Transactions on Vehicular Technology*, vol. 61, no. 3, pp. 1124–1144, March 2012.

[30] A. M. Magableh and M. M. Matalgah, "Moment generating function of the generalized - distribution with applications," *IEEE Communications Letters*, vol. 13, no. 6, pp. 411–413, June 2009.

[31] P. Robertson, E. Villebrun, and P. Hoeher, "A comparison of optimal and sub-optimal map decoding algorithms operating in the log domain," in *Proceedings IEEE International Conference on Communications ICC '95*, vol. 2, June 1995, pp. 1009–1013 vol.2.

[32] J. W. Choi, B. Shim, Y. Ding, B. Rao, and D. I. Kim, "Compressed sensing for wireless communications : useful tips and tricks," *IEEE Communications Surveys Tutorials*, vol. PP, no. 99, pp. 1–1, February 2017.

[33] D. L. Donoho, "Compressed sensing," *IEEE Transactions on Information Theory*, vol. 52, no. 4, pp. 1289–1306, April 2006.

[34] J. Wu and C. Xiao, "Optimal diversity combining based on linear estimation of rician fading channels," *IEEE Transactions on Communications*, vol. 56, no. 10, pp. 1612–1615, October 2008.

[35] M. El-Hajjar and L. Hanzo, "EXIT charts for system design and analysis," *IEEE Communications Surveys Tutorials*, vol. 16, no. 1, pp. 127–153, First 2014.

[36] M. Tuchler, "Design of serially concatenated systems depending on the block length," *IEEE Transactions on Communications*, vol. 52, no. 2, pp. 209–218, Feb 2004.

Siyao Lu received the B.Eng degree in electronic information science and technology from Dalian Maritime University of China and the M.Sc degree from the University of Southampton, U.K., where she is currently pursuing the Ph.D. degree with the Southampton Next Generation Wireless (NGW) Group under the supervision of Prof. L. Hanzo and Dr. M. El-Hajjar. Her research interests mainly include multi-functional MIMO, index modulation, the design of compressed sensing aided transceivers and millimeter wave communications.

Mohammed El-Hajjar is an Associate Professor in the department of Electronics and Computer Science in the University of Southampton. He received his PhD in Wireless Communications from the University of Southampton, UK in 2008. Following the PhD, he joined Imagination Technologies as a design engineer, where he worked on designing and developing Imaginations multi-standard communications platform, which resulted in three patents. He is the recipient of several academic awards and has published a Wiley-IEEE book and in excess of 80 journal and conference papers. Mohammeds research interests include the design of intelligent and energy-efficient transceivers, cross-layer optimization for large-scale networks, MIMO, millimeter wave communications and Radio over fiber network design.

Lajos Hanzo (http://www-mobile.ecs.soton.ac.uk) FREng, F'04, FIET, Fellow of EURASIP, received his 5-year degree in electronics in 1976 and his doctorate in 1983 from the Technical University of Budapest. In 2009 he was awarded an honorary doctorate by the Technical University of Budapest and in 2015 by the University of Edinburgh. In 2016 he was admitted to the Hungarian Academy of Science. During his 40-year career in telecommunications he has held various research and academic posts in Hungary, Germany and the UK. Since 1986 he has been with the School of Electronics and Computer Science, University of Southampton, UK, where he holds the chair in telecommunications. He has successfully supervised 119 PhD students, co-authored 18 John Wiley/IEEE Press books on mobile radio communications totalling in excess of 10 000 pages, published 1800+ research contributions at IEEE Xplore, acted both as TPC and General Chair of IEEE conferences, presented keynote lectures and has been awarded a number of distinctions. Currently he is directing a 60-strong academic research team, working on a range of research projects in the field of wireless multimedia communications sponsored by industry, the Engineering and Physical Sciences Research Council (EPSRC) UK, the European Research Council's Advanced Fellow Grant and the Royal Society's Wolfson Research Merit Award. He is an enthusiastic supporter of industrial and academic liaison and he offers a range of industrial courses. He is also a Governor of the IEEE ComSoc and VTS. He is a former Editor-in-Chief of the IEEE Press and a former Chaired Professor also at Tsinghua University, Beijing. For further information on research in progress and associated publications please refer to http://www-mobile.ecs.soton.ac.uk.